Biochemistry

pubs.acs.org/biochemistry Article

Characterization of Lipidated New Delhi Metallo-β-lactamase Using Synthetic Nanodiscs

Thomas Smisek, Nemanja Vuksanovic, Jada N. Walker, Haily Vu, Dann D. Rivera, Walter Fast, Jennifer S. Brodbelt, and Christian P. Whitman*

Cite This: https://doi.org/10.1021/acs.biochem.5c00106 Read Online

ACCESS | Metrics & More | Article Recommendations | Supporting Information

ABSTRACT: Carbapenem-resistant bacteria present a serious challenge to current treatment methods for bacterial infections. Particularly concerning are metallo-carbapenemases, a subset of plasmid-borne β-lactamases, active against nearly all β-lactam antibiotics and insusceptible to available β-lactamase inhibitors. The most widespread metallo-carbapenemase is New Delhi metallo-β-lactamase (NDM). NDM is unique among all known metallo-β-lactamases due to a post-translational lipidation that anchors it to the outer membrane. Most β-lactamases, including all other metallo-carbapenemases, exist as soluble proteins in the periplasm of Gram-negative bacteria. The functional impact of membrane anchoring remains unclear because most biochemical studies are performed on truncated soluble proteoforms that may have structural and functional differences from the full-length form. To study the functional impact of lipidation, the overexpression of lipidated NDM was optimized in *Escherichia coli* and the lipoprotein was solubilized into synthetic nanodiscs, consisting of lipid bilayer segments encircled by a stabilizing polymer. Highlighting the evolution of metallo-β-lactamases for improved fitness under zinc-limiting conditions, membrane anchoring improves zinc affinity while thermostability is found to be differentially altered in different clinical variants of NDM. These results improve the understanding of the function of a unique membrane-anchored β-lactamase as well as establish a platform for the use of nanodisc-based approaches for the study of bacterial lipoproteins.

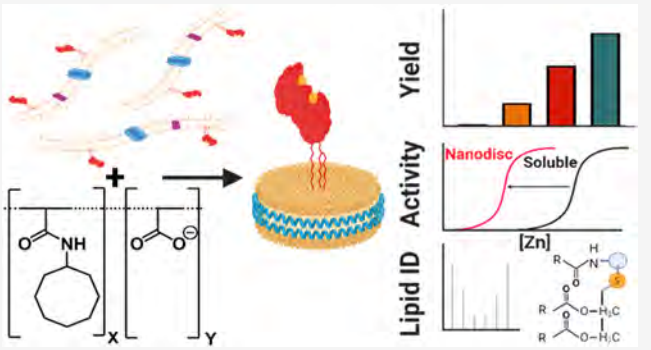

INTRODUCTION

Since their introduction in the 1940s, β-lactam antibiotics remain the most widely used class of antibiotics.[1] Continuous use of β-lactam antibiotics has led to the emergence of several resistance mechanisms including β-lactamases, the main resistance mechanism in Gram-negative bacteria.[2] Resistance to β-lactam antibiotics such as penicillins and cephalosporins led to the development of a new class of synthetic β-lactams, carbapenems, such as imipenem and meropenem, which are currently used as drugs of last resort against multiple drug-resistant infections. The use of carbapenems has spurred the evolution of carbapenemases. Of particular concern are *Klebsiella pneumoniae* carbapenemase (KPC), oxacillinase-48-like carbapenemase (OXA-48), New Delhi metallo-β-lactamase (NDM), Verona integron-encoded metallo-β-lactamase (VIM), and imipenemase (IMP).[2−4] Three of these enzymes, VIM, IMP, and NDM are class-B, metallo-β-lactamases (MBLs). MBLs utilize one or two zinc ions for catalysis in place of the nucleophilic serine present in class A, C, and D serine-β-lactamases (SBLs). Metallo-carbapenemases have broad substrate profiles, degrading all clinically available β-lactam antibiotics except for monobactams, while most serine-carbapenemases have a narrower substrate profile.[5] Perhaps most importantly, while SBLs can be treated with inhibitors that target the serine nucleophile, there are no clinically available inhibitors for MBLs, although several candidates are in clinical trials.[1,6−8]

NDM was first identified in 2008 and has since become the most common metallo-carbapenemase, and the second most common carbapenemase globally.[9] NDM-producing *Enterobacterales*, chiefly *Escherichia coli* and *Klebsiella pneumoniae* have been detected in over 100 countries.[2,10] In the United States, the bla_{NDM} gene was detected in 60% of carbapenem-resistant *E. coli* isolates in 2023.[11] In Gram-negative bacteria, nearly all β-lactamases exist as soluble, periplasmic localized enzymes. NDM however, is a bacterial lipoprotein (BLP) a feature which sets it apart from all known MBLs.[12,13]

BLPs are membrane-bound proteins that are anchored in place via N-terminal acyl moieties. In Gram-negative bacteria

Received: February 25, 2025
Revised: May 20, 2025
Accepted: May 22, 2025
Published: June 3, 2025

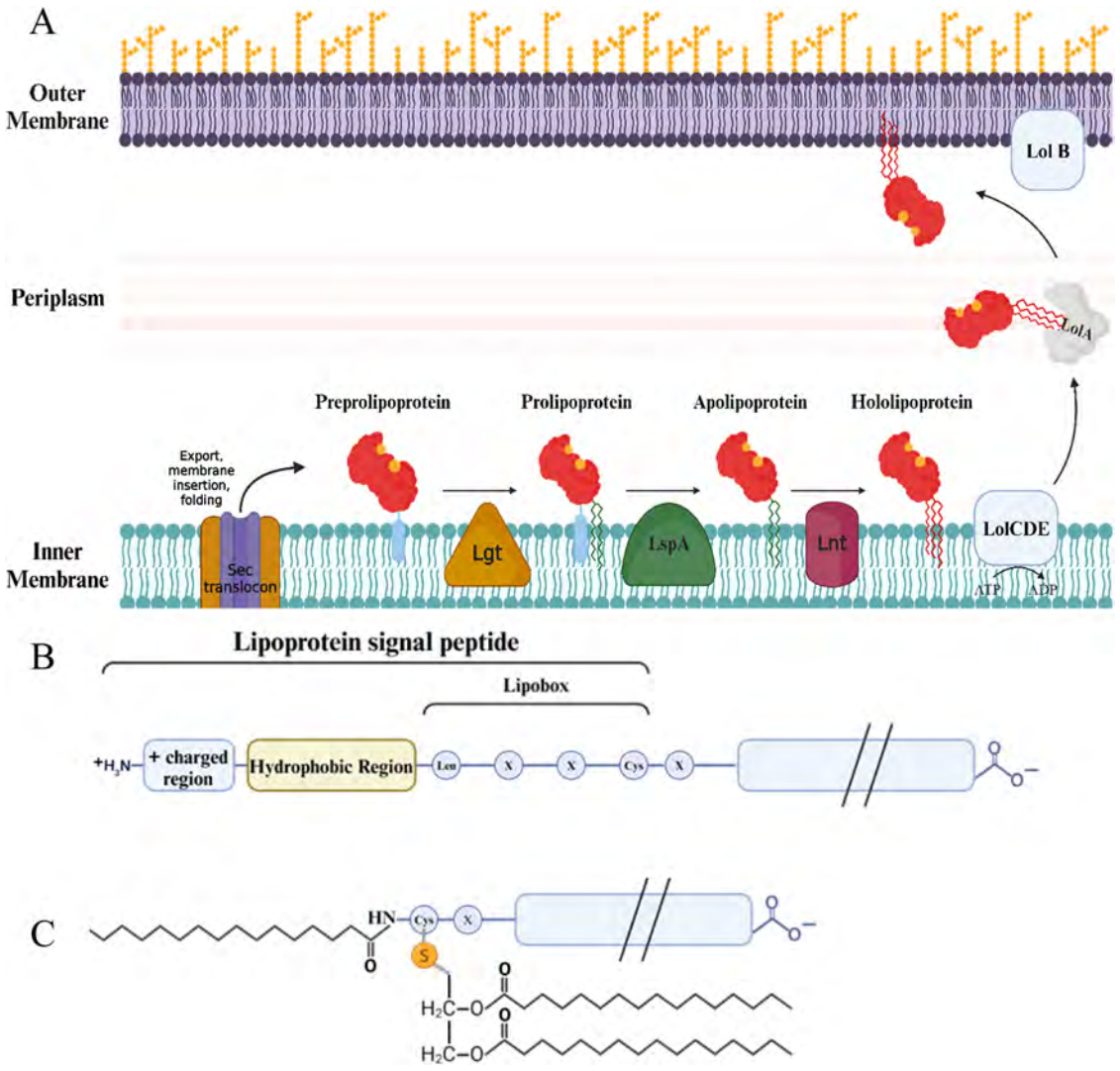

Figure 1. (A) Biosynthetic pathway of bacterial lipoproteins in Gram-negative bacteria. Translocated prelipoprotein is iteratively processed by Lgt, LspA, and Lnt to yield a mature triacylated hololipoprotein (bottom panel). Outer membrane destined lipoproteins are then translocated via the Lol ABCDE system. (B) Composition of lipoprotein signal peptide, consisting of a positively charged N-terminal region, a hydrophobic region, and the lipobox signal sequence. (C) Composition of the modification to a mature triacylated lipoprotein.

such as *Enterobacterales*, lipidation occurs on the inner membrane following export to the periplasm (Figure 1). The prelipoprotein is first anchored via an N-terminal hydrophobic signal peptide that contains a conserved $[LV]^{-3}$ $[ASTVI]^{-2}$ $[GAS]^{-1}$ $[C]^{+1}$ lipidation signal, referred to as a lipobox (LSGC in NDM).[14] A diacylglycerol moiety is then attached to the invariant lipobox cysteine by a thioether linkage, catalyzed by lipoprotein diacyl glyceryl transferase (Lgt), yielding an intermediate prolipoprotein species. Next, the prolipoprotein is cleaved by lipoprotein signal peptidase (LspA/SpII) with the modified cysteine becoming the N-terminal residue. Lipoprotein N-acyl transferase (Lnt) appends a third acyl moiety via amide linkage to the N-terminus, yielding a mature triacylated bacterial lipoprotein (hololipoprotein).[15,16] Outer membrane localized lipoproteins, such as NDM are then exported to the outer membrane via the lipoprotein outer membrane localization (Lol) pathway.[17,18]

While NDM is the most widespread metallo-carbapenemase and the only known example of a lipidated MBL, the impact of lipidation on structure and function has not been fully characterized. NDM has been extensively studied using a variety of synthetic soluble proteoforms that omit the lipidation signal sequence.[19−21] These artificial proteoforms are useful for structural analysis,[12,22] and the development of inhibitors.[23−25] Studies on lipidated NDM, chiefly carried out *in vivo* or via artificially assembled liposomes, suggest differences with regard to enzymatic activity, stability, and binding of zinc.[13,26−28] To bridge the gap between existing studies of lipidated NDM and widely used soluble proteoforms, we developed a method to overexpress and purify the lipidated proteoform of NDM, termed lipo-NDM using synthetic nanodiscs, also known as styrene-maleic acid-like lipid particles (SMALPs). We focused on NDM-1, the most studied variant of NDM, and the clinical variant NDM-15 which in previous studies using soluble proteoforms showed the greatest increase in zinc affinity and thermostability compared with NDM-1.[29] We found that lipo-NDM can be purified in synthetic nanodiscs with yields that are comparable to previous studies on lipoprotein overexpression.[30,31] Careful consideration of growth and purification conditions is required to reduce the production of unwanted nonlipidated proteoforms.[30,32] Lipo-NDM-1 displays comparable enzymatic

https://doi.org/10.1021/acs.biochem.5c00106
Biochemistry XXXX, XXX, XXX−XXX

activity with synthetically soluble constructs, rapidly degrading β-lactams of all major structural classes. In NDM-1, lipidation appears to have no impact on thermostability, while lipo-NDM-15 exhibits a significant increase in stability over a nonlipidated proteoform. Lipidation improves the binding of crucial zinc cofactors in both variants, with 5-fold and 10-fold increases in Zn affinity measured in lipo-NDM-1 and lipo-NDM-15, respectively.[29] Lipidation thus primarily influences zinc affinity, improving fitness in low-zinc environments that occur during infection as a result of nutritional immunity.[33,34]

MATERIALS AND METHODS

Construction of NDM Plasmids. A previously described *E. coli* optimized full-length NDM-1 incorporating a C-terminal 6xHis-tag in a pET-27 vector was used as a template for all full-length NDM variants used in this study.[19] In order to improve purification efficiency, the C-terminal His-tag was replaced with a C-terminal strep-II tag and linker (GGGSGGSAWSHPQFEK) using the Q5 site-directed mutagenesis kit [New England Biolabs (NEB), Ipswich MA] following the manufacturer's instructions. The affinity tag was incorporated on the C-terminus so it would not interfere with the N-terminal signal peptide directing periplasmic export and lipidation. All cloning processes were verified by Sanger sequencing (Eton Biosciences, San Diego, CA). The native NDM-1 signal peptide was replaced by the signal peptide for the *E. coli* lipoprotein LpP (MKATKLVLGAVILGSTLLAGC) using the Q5 site-directed mutagenesis kit (NEB). Construction of the clinical variant NDM-15 which contains two point mutations (M154L and A233V) was carried out using the HiFi site-directed mutagenesis kit (NEB). This process was replicated for both full-length and synthetic soluble proteoforms. For full-length NDM-15, the LpP-NDM-1 chimera was used as a template. For the soluble truncation, a previously described synthetic soluble construct that replaces the first 35 residues of NDM with a PelB periplasmic localization signal peptide was used.[19]

Screening Lysate Fractions for β-Lactamase Activity. Lysate fractions (soluble lysate, total membranes, inner membranes, outer membranes) were resuspended in 50 mM HEPES buffer, pH 7.5, containing 150 mM NaCl, 1 μM $ZnSO_4$, and 1% Tween-20. Total protein content was measured by the Bradford assay and all samples were normalized to a final concentration of 1.0 mg/mL protein. Each sample (10 μL) was diluted to 300 μL in 50 mM HEPES buffer, pH 7.5, containing 150 mM NaCl, 1 μM $ZnSO_4$, 1% Tween-20 and 50 μM Chromacef. β-Lactamase activity was measured by monitoring absorbance at 442 nm.[35] Samples were measured in triplicate.

Expression of Full-Length NDM in Rich Media. *E. coli* BL21(DE3) cells containing the pET-27-NDM-1-His-tag were cultured in 2xYT media containing 50 μg/mL of kanamycin at 37° to an OD_{600} of 0.8. Cells were then cooled to 22 °C and expression was induced by the addition of isopropyl β-D-1-thiogalactopyranoside (IPTG) to 0.5 mM and $ZnSO_4$ to 50 μM. Cells were shaken overnight at 22 °C.

Expression of Full-Length NDM in Minimal Media. *E. coli* C43(DE3) cells containing pET-27-NDM-strep were cultured in M9 or LM9 media supplemented with 50 μg/mL kanamycin at 37 °C for ∼5.5 h to an OD_{600} of 0.8 and then cooled to 22 °C followed by the addition of IPTG to 0.5 mM and $ZnSO_4$ to 50 μM. Cells were shaken overnight at 22 °C.

Initial Outer Membrane Fractionation. Cells grown in 2xYT media were lysed by sonication (Fisher Scientific Model-500 Sonic Dismembrator) and membranes were collected by centrifugation at 50,000*g* for 1 h at 4 °C. The total membrane fraction was washed with TRIS buffer pH 7.5 and suspended in TRIS buffer to a final concentration of 50 mg/mL. N-lauroylsarcosine was then added to 2% w/v and incubated for 1 h at ambient temperature. To separate the inner membrane (IM) and outer membrane (OM) fractions, the suspension was centrifuged at 100,000*g* for 1 h at 4 °C. Pellets were then washed and resuspended in 50 mM HEPES buffer, pH 7.5, 300 mM NaCl, 1 μm ZnSO4, 10% glycerol to 100 mg/mL.

Spheroplast and Total Membrane Preparation. All steps were conducted at 4 °C unless otherwise noted. Cells expressed in minimal media were harvested by centrifugation at 7500*g* for 10 min. Cells were converted to spheroplasts by suspension in 50 mM TRIS buffer, pH 8.0, containing 500 mM sucrose, 0.75 mM EDTA, and 0.2 mg/mL lysozyme. Cells were incubated on a shaker plate for 30 min before being centrifuged for 15 min at 10,000*g*. The resultant pellet was then washed 3 × with 50 mM TRIS buffer, pH 8.0, containing 200 mM Sucrose, 1 mM $MgCl_2$, 5 μM $ZnSO_4$, and resuspended in the same buffer with the addition of a Pierce complete protease inhibitor cocktail, EDTA free (Thermo Fisher Scientific, Waltham, MA). Spheroplasts were lysed by French press (2 passages at 16,000 psi), and the resultant homogenate was clarified by centrifugation for 15 min at 10,000*g* to remove any unbroken cells. Total membranes were collected by ultracentrifugation of the clarified homogenate for 2 h at 100,000*g*. Membranes were resuspended to 400 mg/mL in 50 mM TRIS buffer, pH 8.0, containing 1 μM $ZnSO_4$ and homogenized by repeated gentle passage through an 18-gauge needle.

Outer Membrane Enrichment. All steps were conducted at 4 °C unless otherwise noted. The total membrane suspensions (400 mg/mL) were diluted 1:1 with 50 mM TRIS buffer, pH 8.0, containing 1% N-lauroylsarcosine, and incubated on a shaker plate for 1 h. The suspension was then ultracentrifuged for 1 h at 100,000*g*. The pellet, representing the sarkosyl-insoluble OM fraction was resuspended in 50 mM HEPES buffer, pH 7.5, containing 300 mM NaCl and 1 μM $ZnSO_4$, and incubated 15 min on a shaker plate before being ultra centrifuged 15 min (150,000*g*). The final washed outer membrane pellet was resuspended to 100 mg/mL in 50 mM HEPES buffer, pH 7.5, containing 1 μM $ZnSO_4$, 300 mM NaCl, and 15% glycerol. The mixture was then snap frozen in liquid N_2. Typical yields were 300−400 mg of OM per 1 L of cell culture. OM suspensions were stored for up to 3 months at −80 °C with no significant loss of β-lactamase activity. Separation of IM and OM was assessed by an NADH dehydrogenase activity.[36]

Screening of Synthetic Nanodisc-Forming Polymers. Commercially available Acrylic Acid CoStyrene (AASTY), CyclAPol, and diisobutylenemaleic acid (DIBMA) nanodisc-forming polymers were purchased from Cube Biotech (Monheim am Rhein, Germany) and stored at −20 °C. Stocks were reconstituted to 10% w/v in Milli-Q H_2O and incubated 30 min at room temperature with gentle agitation. Membrane fractions purified from BL21(DE3) were thawed and diluted in 50 mM HEPES buffer, pH 7.5, containing 1 μM $ZnSO_4$, and 300 mM NaCl. In separate tubes, aliquots of polymer were added to a final concentration between 0.1−2.5%. Samples were incubated at 4 °C overnight and centrifuged for 1 h at

https://doi.org/10.1021/acs.biochem.5c00106
Biochemistry XXXX, XXX, XXX−XXX

20,000*g*. Solubilization was assessed by SDS-PAGE and a β-lactamase activity assay. Prior to SDS-PAGE samples were separated from excess polymer via precipitation.[37] Prior to activity measurements, samples were buffer-exchanged to remove excess polymer.

Solubilization of Lipidated NDM-1 Using DIBMA-Glycerol. DIBMA-Glycerol powder stocks were reconstituted, as stated above. Aliquots of a 100 mg/mL outer membrane suspension were thawed on ice. Polymer and membrane suspensions were combined and diluted to a final concentration of 2.5% w/v and 25 mg/mL, respectively, in solubilization buffer (50 mM HEPES buffer, pH 7.5, containing 1 μM $ZnSO_4$, and 300 mM NaCl). The solubilization mixture was incubated at 4 °C overnight with a constant inversion. Following incubation, the mixture was ultracentrifuged for 30 min at 100,000*g*, 4 °C to remove insoluble materials.

Solubilization of Lipidated NDM Using Ultrasolute CyclAPol. CyclAPol powder stocks were reconstituted, as described above. Outer membrane suspension aliquots (100 mg/mL) were thawed on ice. Polymer and membrane suspensions are combined and diluted to a final concentration of 0.1% w/v and 10 mg/mL, respectively, in solubilization buffer (50 mM HEPES, pH 7.5, containing 1 μM $ZnSO_4$, 300 mM NaCl, and 10% glycerol). The solubilization mixture was then incubated at 4 °C overnight with constant inversion. Following incubation, the mixture was ultracentrifuged for 1 h at 100,000*g*, 4 °C to remove insoluble materials. To remove unbound polymer as well as any residual soluble proteins the mixture was concentrated and buffer exchanged into purification buffer to a volume of 20 mL. Buffer exchange was carried out using a vacuum concentrator fitted with a 100 kDa MWCO membrane filter. Flowthrough was tested for β-lactamase activity. If the 100 kDa flowthrough was found to contain significant activity (>10% of the activity of the 100,000*g* supernatant sample) the purification sample was discarded.

Purification of Strep-Tagged Nanodisc-solubilized NDM. The concentrated supernatant was applied to 2.0 mL of streptactinXT-4flow resin (IBA Lifesciences Göttingen, Germany) at 4 °C overnight with constant inversion. The mixture was then transferred to a gravity column, and the resin was allowed to settle. The supernatant was then allowed to pass through the resin and was collected as flowthrough. The column was washed with 10 column volumes of column-wash buffer (50 mM HEPES buffer, pH 7.5, containing 5 μM $ZnSO_4$). NDM-containing nanodiscs were eluted using column-elution buffer (50 mM HEPES buffer, pH 7.5, containing 5 μM $ZnSO_4$ and 50 mM biotin). Elution fractions containing protein were pooled and buffer exchanged using a 100 kDa spin column. The purified nanodisc-bound protein was concentrated to a final concentration of 100 μM in Nanodisc storage buffer (50 mM HEPES, pH 7.5, containing 5 μM $ZnSO_4$ and 25% glycerol) and snap-frozen in liquid N_2. Nanodisc-protein aliquots were stored at −80 °C.

Purification of His-Tagged Nanodisc-Solubilized NDM. The 100,000*g* supernatant was applied to 4.0 mL of Ni-NTA resin (Thermo Fisher Scientific) at 4 °C overnight with constant inversion. The mixture was transferred to a gravity column and the resin was allowed to settle. The supernatant was then allowed to pass through the resin and collected as flowthrough. The column was washed with 5 column volumes of wash buffer A (50 mM HEPES buffer, pH 7.5, containing 5 μM $ZnSO_4$, and 300 mM NaCl) followed by 5 column volumes of wash buffer B (50 mM HEPES buffer, pH 7.5, containing 1 μM $ZnSO_4$, 300 mM NaCl, and 10 mM imidazole). NDM-containing nanodiscs were eluted using column-elution buffer (50 mM HEPES buffer, pH 7.5, containing 1 μM $ZnSO_4$, 300 mM NaCl, and 10 mM Imidazole). Elution fractions containing protein were pooled and buffer exchanged by using a 10 kDa spin column. The purified nanodisc-bound protein was concentrated to a final concentration of 100 μM in (50 mM HEPES, pH 7.5, containing 5 μM $ZnSO_4$, 300 mM NaCl, and 25% glycerol) and snap frozen in liquid nitrogen. Nanodisc-protein aliquots were stored at −80 °C.

Purification of Soluble Truncated Proteoforms from the Expression of Full-Length NDM-1. Mixed membrane fractions obtained from sonication of cells grown in rich media were resuspended to 200 mg/mL in 50 mM HEPES, pH 7.5, containing 1 μM $ZnSO_4$, and 300 mM NaCl and homogenized by passage through an 18-gauge needle. The suspension was then incubated for 15 min on a shaker plate before being centrifuged for 1 h at 100,000*g*. An aliquot (10 μL) of the supernatant was diluted to 300 μL in 50 mM HEPES buffer, pH 7.5, containing 50 μM chromacef to test for β-lactamase activity. The washed mixed membranes were resuspended in solubilization buffer (50 mM HEPES, pH 7.5, containing 1 μM $ZnSO_4$, 300 mM NaCl, and 10% glycerol) and diluted with either DIBMA-glycerol or CyclAPol to a final concentration of 0.1% w/v CyclAPol, 10 mg/mL membranes or 2.5% DIBMA-Gly, 25 mg/mL membranes, respectively, in solubilization buffer. The solubilization mixture was then incubated at 4 °C overnight with constant inversion. Following incubation, the mixture was ultracentrifuged for 1 h at 100,000*g*, 4 °C to remove insoluble materials. Strep-tag affinity purification was carried out as described above. Buffer exchange and concentration steps using either spin concentrators or pressure concentrators used filters with MWCO values of 10 kDa. To separate soluble truncations from trace nanodisc-bound proteoforms, this process was repeated with a 100 kDa MWCO filter.

Purification of Synthetic Soluble NDM Variants. Soluble NDM-1 and NDM-15 were purified as described previously using a truncation that omits the first 35 residues, including the lipidation signal peptide, and inserts a PelB leader sequence to drive periplasmic localization.[19,29]

Native PAGE Analysis. Nanodisc-protein particle size was estimated by migration on a nondenaturing native PAGE gel.[38] A 20 μM sample of purified nanodisc sample was loaded onto a 4−10% native PAGE gel and run for 3 h at 150 V, 4 °C. The molecular weight of the sample was estimated by comparison to the migration of the Native Mark protein standard (ThermoFisher) as well as migration of a purified soluble NDM-1 truncation.

Dynamic Light Scattering. For light scattering experiments, samples were analyzed using a DAWN HELEOS-II multiangle light scattering photometer with an Optilab T-rex refractometer detector and a Wyatt QELS dynamic light scattering detector (MALS-QELS system; Wyatt Technology, Santa Barbara, CA). Samples were delivered to the detector following passage through a TSK-GEL $G300PW_{XL}$ size-exclusion column (7.8 mm × 300 mm, pore size of 300 Å) (Tosoh Bioscience LLC, King of Prussia, PA) connected to a Shimadzu LC-20AD HLPC system (model WTC-030S5). The mobile phase consisted of 50 mM HEPES buffer, pH 7.5, 150

https://doi.org/10.1021/acs.biochem.5c00106
Biochemistry XXXX, XXX, XXX−XXX

mM NaCl, and 1 μM $ZnSO_4$ with a flow rate of 0.4 mL/min. Prior to the analysis all samples were filtered through a 1 mDa MWCO filter, dialyzed overnight in the mobile phase and diluted to a final concentration of 50 μM. Samples were injected in 20 μL portions. Mass fractions, polydispersity, hydrodynamic radius, and molar mass were determined using Astra-6 software (Wyatt Technology).

Top−Down Mass Spectrometry. Purified nanodisc NDM-1 was desalted and exchanged into water by using a Micro Bio-Spin *P6* gel column (BioRad Laboratories Inc., Hercules, CA). The sample was diluted to ∼2 μM in a solution of 50/49.5/0.5 (v/v/v) methanol/water/formic acid and electrosprayed at 2 μL/min using an applied voltage of 3.0 kV. All analyses were performed on a Thermo Fisher Scientific Orbitrap Eclipse mass spectrometer (Bremen, Germany), modified with an Excistar 193 nm ArF excimer laser (Coherent, Santa Cruz, CA) to enable ultraviolet photodissociation (UVPD) in the high-pressure linear ion trap. Mass spectra were collected at 120,000 resolution (defined at m/z 200) using a scan range of m/z 500−2000, automatic gain control (AGC) target of 1E6, and maximum injection time of 50 ms. For MS/MS analysis involving UVPD, a single charge state of each proteoform was quadrupole-isolated by using a width of 1.3 m/z and activated by using a single 0.75 mJ laser pulse. Fragment ions generated by UVPD were isolated using windows spanning m/z 466.6−966.6 (lower m/z window) and m/z 996.6−1496.6 (higher m/z window) for lipid−NDM-1 proteoform 1 (precursor m/z 976.6, 29+) and m/z 467.6−967.6 (lower m/z window) and m/z 1007.6−1507.6 (higher m/z window) for lipid NDM-1 proteoform 2 (precursor m/z 977.6, 29+) and subjected to proton transfer charge reduction (PTCR) using perfluoroperhydrophenanthrene (PFPP) as the PTCR reagent (AGC target of 2E) and a reaction time of 7 ms (MS^3). Additional fragment ions of interest were reisolated for MS^4 analysis and subjected to higher-energy collisional dissociation (HCD) using a normalized collision energy (NCE) of 35%. All MS^n spectra, corresponding to 100−200 transient averages, were collected at 240,000 resolution (defined at m/z 200) using scan ranges between m/z 200−4000, AGC target of 1E6, and maximum injection time of 500 ms. Easy-IC (internal calibration) was utilized for enhanced mass accuracy of detected fragment ionsAll spectra were deconvoluted using the Xtract algorithm within Thermo Fisher Scientific FreeStyle version 1.8. The following deconvolution parameters were used: fit factor of 70%, remaining threshold of 25%, and signal-to-noise (S/N) threshold of 10. Sequence ions were identified using MS-TAFI[39] and ProSight Lite software set to search for ion types generated by UVPD (*a*, *a*+1, *b*, *c*, *x*, *x*+1, *y*, *y*−1, and *z*) within a fragment mass tolerance of ±10 ppm. Sequence ions discovered in two out of three replicates were retained for the final calculation of sequence coverage and proteoform scores following UVPD and UVPD/PTCR. Top-down mass spectrometry of purified soluble NDM-1 truncations was performed as described previously.[40]

Preparation of Mono-Zn Enzyme (NDM-1,15). An aliquot of purified nanodisc-bound NDM-1 (100 μM) or soluble NDM-1/15 (100 μM) was buffer exchanged into 50 mM HEPES, pH 7.5, 150 mM NaCl, and 1 mM tris(2-carboxyethyl)phosphine (TCEP) using a 10 kDa MWCO Amicon spin column (100 kDa for nanodisc-NDM-1). Zinc content was measured under denaturing conditions to verify that the sample contained 1.9−2.0 equiv of zinc. The sample was then diluted to 10 μM with the addition of 4-pararesorcinol (PAR) to a final concentration of 100 μM. The mixture was transferred to a quartz cuvette and placed in a spectrophotometer at room temperature. Absorbance was continuously monitored at 500 nm until it reached a value corresponding to a 10 μM Zn-PAR complex as measured by a standard curve, indicating that one Zn ion had been chelated per enzyme molecule. The sample was then cooled to 4 °C and buffer exchanged into 50 mM HEPES buffer, pH 7.5, and 1 mM TCEP until measured absorbance at 500 nm was comparable to a blank solution indicating that all PAR had been removed. The amount of Zn present in the sample was quantified under denaturing conditions to confirm that ∼1.0 equiv of zinc ion per protein molecule, and the sample was assayed for β-lactamase activity in the absence of exogenous zinc to verify the lack of activity.

Preparation of Mono-Zn Nanodisc-NDM-15. An aliquot of purified nanodisc-bound NDM-15 (100 μM) was buffer exchanged into 50 mM HEPES, pH 7.5, 150 mM NaCl, and 1 mM TCEP using a 100 kDa MWCO Amicon spin column. Zinc content was measured under denaturing conditions to verify that the sample contained 1.9−2.0 equiv of zinc. Approximately 250 mg of Chelex resin (Biorad) equivalent to a column volume of 0.4 mL was washed with 4 mL of 50 mM HEPES, pH 7.5, 150 mM NaCl, and 1 mM TCEP. The washed nanodisc-NDM-15 sample was then applied to the Chelex resin and incubated for 1 min at ambient temperature. The protein was then eluted from the column by washing it with 2 mL of buffer. Pooled elutions containing protein as measured by Bradford assay were buffer exchanged into 50 mM HEPES, pH 7.5, and made 1 mM TCEP and concentrated to 100 μM. The amount of Zn present in the sample was quantified under denaturing conditions to confirm that approximately 1.0 equiv of zinc ion per protein molecule. The sample was assayed for β-lactamase activity in the absence of exogenous zinc to verify the lack of activity.

Zn Concentration Dependence of Ampicillin Hydrolysis. The effect of Zn concentration of hydrolysis was assayed as previously reported.[29] Quartz microcuvettes were soaked in 0.01% Tween-20 overnight and washed extensively with milli-Q-treated water and ethanol. Mono-Zn NDM was then assayed for ampicillin hydrolysis repeatedly in Zn-free buffer until a consistent minimal baseline level of absorbance change at 235 nm was established that did not exceed 5% of the activity of a di-Zn sample measured in a separate cuvette with 1 μM exogenous Zn. The final assay conditions were 50 mM HEPES, pH 7.0, 600 μM ampicillin, and 20 nM enzyme (NDM-1 or soluble NDM-15) or 5 nM enzyme (nanodisc NDM-15). Zn concentrations assayed ranged from 1 nM to 100 μM. To avoid Zn contamination, all buffers were pretreated with Chelex-100 resin (Biorad) to remove any trace metal ion contaminants, and Zn concentrations were tested from lower to higher concentrations. Rates of ampicillin hydrolysis were converted to percentages of the maximum rate observed. To determine binding of Zn-2% activity vs [Zn] was fit using eq 1 as previously described.[29]

$$\%\ \text{activity} = (x + ((100 - x)/(1 + [\text{Zn}]/y) + (z/[\text{Zn}])))) \quad (1)$$

In this equation, [Zn] is the concentration of $ZnSO_4$, x is the activity rate with no added zinc and Y is the K_d of Zn-2, Z is the K_d for the binding of the inhibitory Zn-3.[41]

https://doi.org/10.1021/acs.biochem.5c00106
Biochemistry XXXX, XXX, XXX−XXX

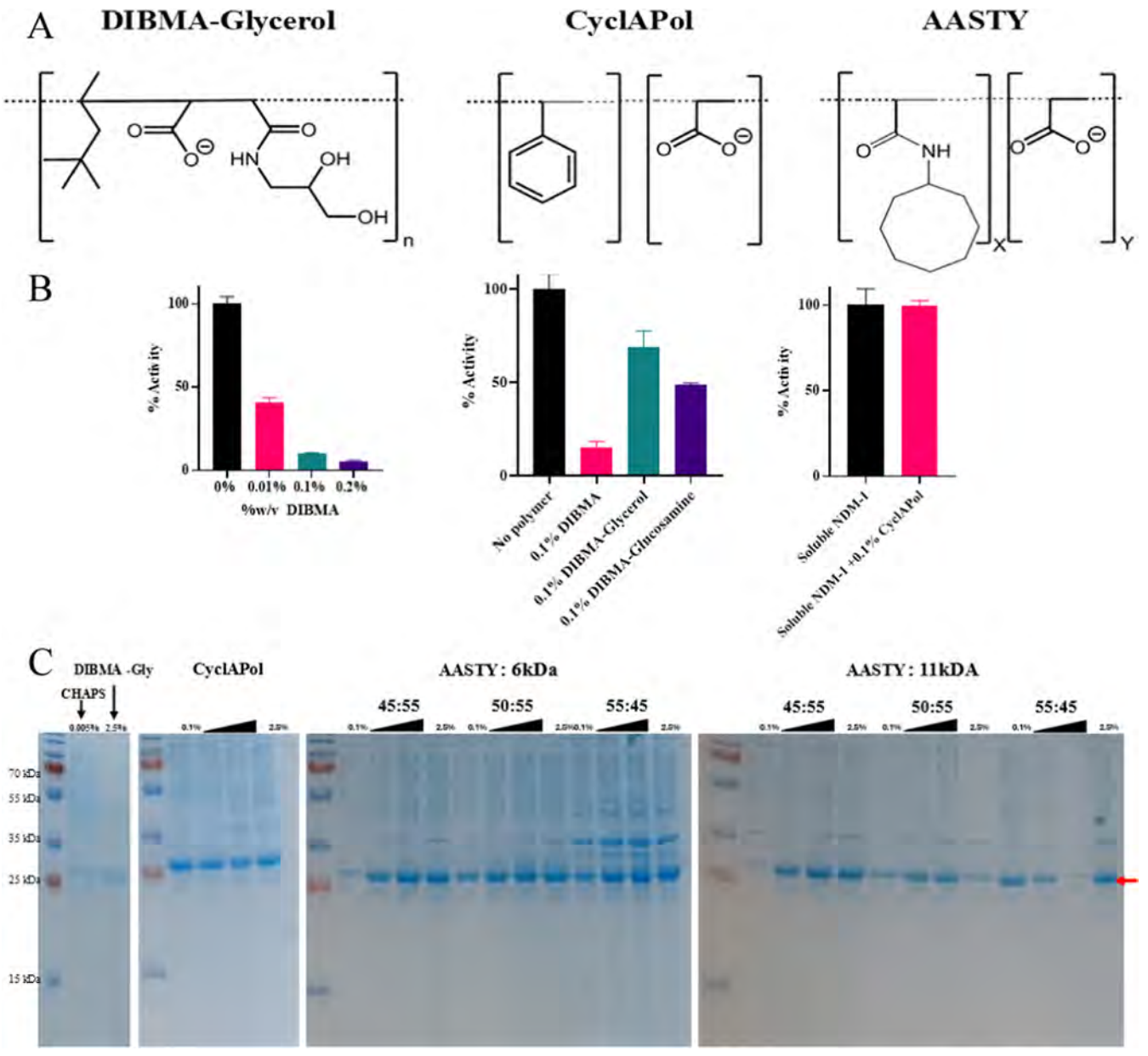

Figure 2. (A) Composition of Nanodisc-forming polymers used. *X* and *Y* indicate the ratios of polymer subunits. AASTY variants studied included 45:55, 50:50, and 55:45 ratios. Six and 11 kDa correspond to the average molecular weight of the AASTY variant reflecting differences in the chain length. (B) Inhibition of soluble NDM-1 by free DIBMA polymer variants and CyclAPol. (C) Solubilization screen of NDM-1 (red arrow) by diisobutylenemaleic acid-glycerol (DIBMA-glycerol), acrylic acid costyrene (AASTYs), and CyclAPol C8−C0−50 polymers. Acrylic acid-based polymers were screened at concentrations of 0.1, 0.5, 1.0, and 2.5% w/v.

Nanodifferential Scanning Fluorimetry (nanoDSF). All NDM-1 and NDM-15 samples were analyzed using nanoDSF at an enzyme concentration of 10 μM. The analyses of dizinc samples were carried out in 50 mM HEPES buffer (pH 7.5) containing 10 μM $ZnSO_4$ and 20% glycerol. Samples were incubated on ice for 30 min prior to the measurements. A heating rate of 2.0 °C/min was applied over a temperature range of 20−95 °C. Samples were analyzed by using excitation at 280 nm, and melting points were determined by taking the first derivative of the fluorescence emission intensity ratio (350/330 nm).

Steady-State Kinetics. For all substrates measured, assay conditions were: 50 mM HEPES, pH 7.0, with 1 μM $ZnSO_4$ unless stated otherwise. Absorbance changes due to hydrolysis of substrate were measured for 0.3 min at room temperature in a quartz microcuvette. The concentration of enzyme varied from 5−20 nMol and was adjusted to ensure the rate of change of absorbance remained linear during each measurement. Substrates were measured at the corresponding wavelength (Table S1). Steady-state rate constants are determined by fitting initial rate values against substrate concentration using GraphPad Prism version 10.0.2 (GraphPad Software).

RESULTS

Selection of Nanodisc-Forming Polymers. Most synthetic nanodisc-forming polymers consist of alternating maleic acid and cyclic aromatic units. Dicarboxylic acid motifs like maleic acid are known zinc chelators,[23] requiring a focus on nondicarboxylic acid-containing polymers. This initially constrained us to diisobutylenemaleic acid (DIBMA) variants

https://doi.org/10.1021/acs.biochem.5c00106
Biochemistry XXXX, XXX, XXX−XXX

Table 1. Approximate Yields of Nanodisc-Bound Protein under Different Conditions[a]

protein construct	strain	polymer	growth media	yield/g of OM	yield/L (culture)
L-NDM	BL21(DE3)	DIBMA-Gly	LB	200 μg	50 μg
L-NDM	BL21(DE3)	Amphi-18	LB	N.D.	~500 μg
L-NDM	C43(DE3)	Amphi-18	M9	N.D.	N.D.
LpP-NDM	C43(DE3)	Amphi-18	M9	4 mg	1.3 mg
LpP-NDM	C43(DE3)	Amphi-18	LM9	6 mg	2.0 mg

[a]Cell culture (1 L) corresponds to ~0.3 g of isolated OM.

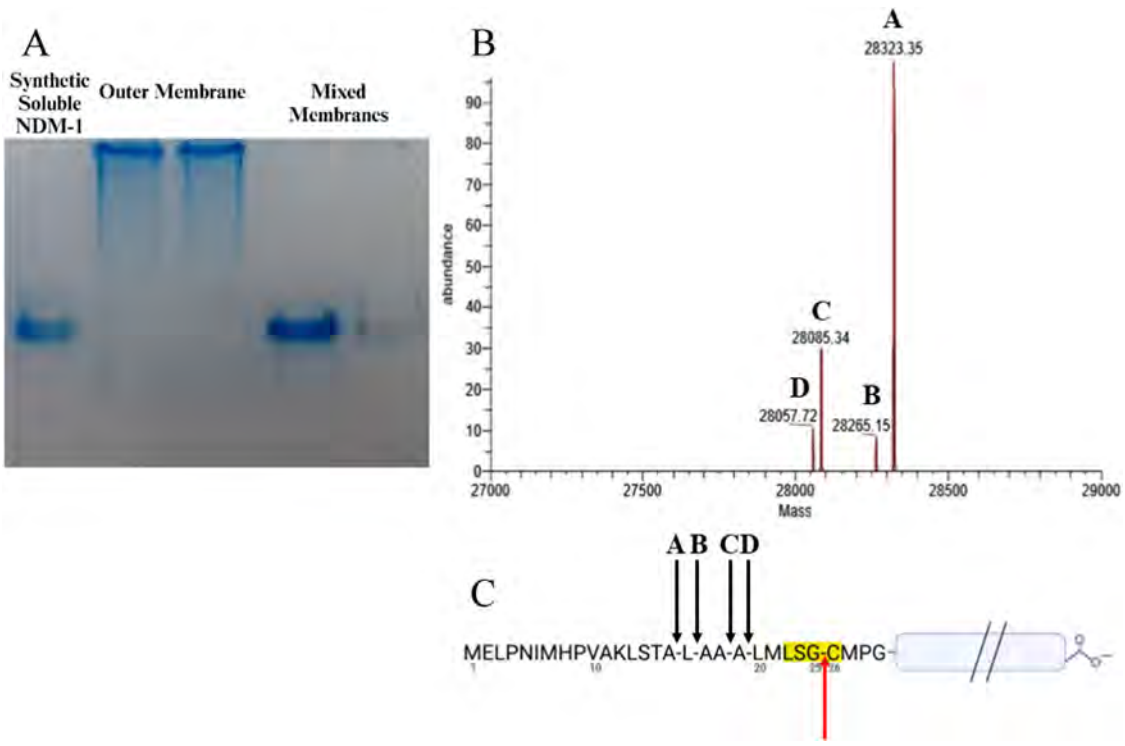

Figure 3. (A) Purified NDM solubilized from mixed membrane and outer membrane fractions visualized on native PAGE Gel in comparison to purified 25 kDa synthetic soluble NDM-1. (B) Top-down LC-MS analysis of purified soluble NDM-1 obtained from mixed membrane solubilization. (C) NDM-1 signal peptide with a predicted lipidation cut site (red) and predicted cleavage sites corresponding to detected soluble proteins.

(Figure 2A), of which DIBMA-Glycerol showed the least inhibitory effect on NDM activity (Figure 2B). Due to low yields, we screened a library of more recently commercially available nanodisc-forming polymers, belonging to 2 classes: acrylic acid costyrene (AASTY), and cycloalkane amphipols (CyclAPol) (Figure 2A), which showed no inhibitory effect on NDM activity (Figure 2B). Screening showed that CyclAPol C8−C0−50 and AASTY 6 kDa variants dramatically outperformed DIBMA-Glycerol (Figure 2C − red arrow). CyclAPol and AASTY 6 kDa variants improved purified protein yields from 50 μg to 300−500 μg per liter of cell culture compared to DIBMA-glycerol. CyclAPol C8−C0−50, CyclAPol for brevity, sold as Ultrasolute Amphipol-18 (Cube Biotech no. 18321), was selected due to lack of UV absorbance by the polymer, simplifying protein quantification and compatibility with UV−vis based enzymatic activity assays.

Solubilization of Lipo-NDM. Several different parameters were investigated (expression conditions, various media, and different *E. coli* strains, non-native signal peptide) in order to optimize the yield of nanodisc-bound protein (lipidated NDM). Recombinant full-length NDM-1 was expressed in *E. coli* strain Bl21(DE3). An outer membrane (OM) fraction was extracted by N-lauroylsarcosine treatment of the insoluble lysate.[42,43] The resulting outer membrane (OM)-enriched fraction was then coincubated with either DIBMA-Glycerol or CyclAPol at polymer: membrane ratios from 1:1 to 1:10. Following incubation and separation of soluble and insoluble fractions by ultracentrifugation, analysis of the soluble fraction showed that it displayed 1000-fold higher β-lactamase activity than an insolubilized sample and a major band corresponding to NDM (27 kDa, as assessed by SDS-PAGE), which was not present in a nonpolymer treated membrane sample. Polymer-solubilized NDM-1 could be easily purified following solubilization by using routine affinity chromatography techniques. However, due to low yields, less than 0.5 mg of purified protein per liter of cell culture using CyclAPol, the expression conditions were optimized to improve yield (Table 1).

Overexpression of Full-Length NDM-1 Causes Accumulation of Nonmembrane-Bound Proteins. During OM enrichment, analysis by β-lactamase activity and SDS-PAGE showed that the majority of membrane-bound NDM was retained in the inner membrane (IM) fraction along with significant amounts present in the soluble lysate. Solubilization

https://doi.org/10.1021/acs.biochem.5c00106
Biochemistry XXXX, XXX, XXX−XXX

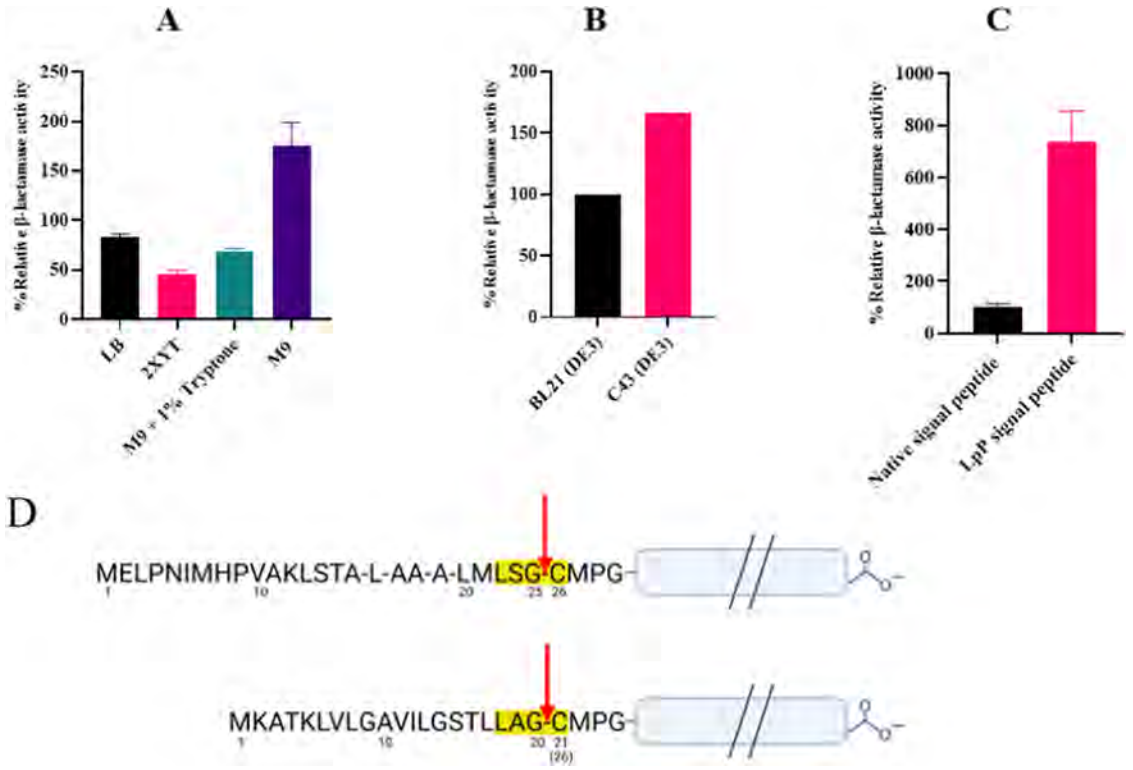

Figure 4. (A) Relative β-lactamase activity of the total membrane fraction in comparison to the activity of the soluble fraction following lysis of NDM-1 expressing *E. coli* were grown in various growth media. (B) Increase in total membrane localized β-lactamase activity when expressed in C43(DE3) compared to BL21(DE3). (C) Increase in OM-localized β-lactamase activity following substitution of the native NDM signal peptide with the signal peptide from *E. coli* lipoprotein LspA. (D) Amino acid composition of the native signal peptide (top panel) and the LpP signal peptide (bottom panel) with the LspA cleavage site marked in red. Black indicates predicted cut sites corresponding to soluble proteoforms.

of a total membrane fraction was investigated to increase yield, with the intention of separating mature lipoprotein (i.e., the hololipoprotein) from precursors (Figure 1A). Unexpectedly and despite repeated wash steps prior to solubilization to remove nonmembrane-bound contaminants, total membrane solubilization, and purification produced a heterogeneous NDM sample containing trace amounts of nanodisc-bound protein (Figure 3A), but primarily consisting of a soluble truncated proteoform with an apparent molecular mass of 25−30 kDa that could be easily differentiated from nanodisc-bound protein by native PAGE (Figure 3A) and isolated using a 100 kDa Molecular Weight cutoff (MWCO) ultrafiltration device.

The truncated proteoform was analyzed by liquid chromatography−mass spectrometry (LC-MS) (Proteomics Core Facility, University of Texas at Austin) to determine the molecular masses of the truncated proteoforms. LC-MS analysis determined that the sample consisted of a heterogeneous mixture with molecular masses of 28 058, 28 085, 28 265, and 28 323 Da, (Figure 3B) consistent with cleavage after residues 16, 17, 19, and 20 (Figure 3C). The identified cleavage sites align with recognition sites of Signal Peptidase I (SpI), an inner membrane-bound signal peptidase that cleaves following a conserved AxA motif (Figure S1).[44,45] Notably, the NDM signal peptide contains an alanine-rich region containing overlapping AxA motifs between residues 15 and 20. Since solubilization from a washed, OM-enriched fraction yielded no non-nanodisc-bound NDM contaminants, we focused on improving the OM-localized protein yield.

Alteration of Expression Conditions Improves Lipoprotein Yield and Outer Membrane Localization. Lipoprotein expression in minimal media has been previously demonstrated to drastically improve the yield of mature lipidated protein over nonlipidated proteoforms in *E. coli*.[30] Consistent with this observation, the total membrane fraction obtained from cells expressing full-length NDM-1 in M9 showed double the activity of the soluble fraction when normalized for the total protein content. In cells grown in 2xYT, or M9 with amino acid supplementation, the soluble fraction displayed double the activity of the insoluble fraction (Figure 4). The minimal media recipe used in this study was modified from the reference formula for M9 minimal media to increase buffering capacity and glucose content to improve protein yields and cell growth times.[30,46] The modified minimal medium, termed Lipoprotein M9 minimal medium (LM9), doubles the buffering capacity and increases the glucose content from 0.4−0.8 % w/v (Table S2). When *E. coli* C43(DE3), a strain commonly used for expression of both toxic and integral membrane proteins, was found to increase membrane localized activity in M9 by 70% in LM9 media compared to expression using *E. coli* BL21(DE3) (Figure 4C).

Non-native Signal Peptides Reduce Soluble Protein Accumulation. To reduce apparent SpI cleavage and improve OM localization following the detection of unwanted soluble proteoforms, the native NDM signal peptide was replaced with the signal peptide from the structural lipoprotein LpP, also known as Braun's Lipoprotein (Uniprot Accession code: P69776) which does not contain AxA SpI recognition sites (Figure S2). Comparison of the β-lactamase activity of cells expressing either full-length NDM-1 or the LpP-NDM-1

https://doi.org/10.1021/acs.biochem.5c00106
Biochemistry XXXX, XXX, XXX−XXX

chimera showed a 7-fold increase in OM-localized activity (Figure 4C).

Optimized Growth Conditions Enable Efficient Overexpression of Lipidated NDM. Expression of the LpP-NDM chimera in LM9 media yielded 5−6 mg of purified nanodisc-bound protein per gram of outer membrane solubilized equivalent to 1.5−2.0 mg/L protein of cell culture (Table 1, Figure S3). The final sample is free of any detectable soluble proteoforms and was determined to be homogeneous by LC-MS and DLS.

Dynamic Light Scattering. To determine the size distribution of the purified nanodisc sample, Dynamic Light Scattering (DLS) was carried out. Light scattering analysis of purified NDM in CyclAPol nanodiscs showed a single monodisperse species with a molar mass of 311 kDa and a hydrodynamic radius of 21 nm, (Table 2).

Table 2. Parameters Determined by Dynamic Light Scattering (DLS) for Nanodisc-Bound and Synthetically Soluble NDM-1

	nanodisc-NDM-1	soluble NDM-1
molecular weight	311 kDa	25 kDa
polydispersity	1.0	1.0
radius	20.8	N.D.[a]

[a]N.D. not determined.

MS Analysis of Purified Nanodisc-Bound Protein. To confirm the presence of lipidation in purified nanodisc-bound NDM-1, the sample was subjected to top−down mass spectrometry (TD-MS). MS analysis revealed that the purified protein contained two dominant species with molecular weights of 28,277 and 28,305 Da and mass differences of +786 and +814 Da from the predicted mass of C26 N-terminal NDM-1 (Figure S4). The protein was then subjected to ultraviolet photodissociation (UVPD) for MS/MS characterization (Figures 5 and S5). UVPD produced fragment ions encompassing the N-terminal cysteine residue that was determined to be modified by C16:0/C16:1 lipids for the 28,277 Da proteoform (+786 Da modification) and C16:0/C18:1 lipids for the 28,305 Da proteoform (+814 Da modification).

Steady-State Kinetics. The k_{cat} and K_m values for six substrates belonging to the three major structural classes of β-lactams were determined for nanodisc-bound NDM-1 (Table 3). To ensure maximal activity, analysis was carried out in the presence of exogenous zinc. Previously studied soluble truncations of NDM display maximal activity at 10 μM zinc.[19] For lipidated NDM-1 maximal activity was determined to be at 1 μM (*vide infra*). As with soluble truncations of NDM-1, all three classes of β-lactams tested were effectively degraded by lipidated NDM-1 with k_{cat}/K_m values of 1×10^6 M^{-1} s^{-1}. Compared with soluble NDM-1 there is less disparity of K_m values between carbapenems (meropenem, imipenem) and penams (penicillin-G, ampicillin), while cephems (cephalexin, cefaclor) displayed K_m values 10-fold lower than those for other classes. Like soluble NDM-1, these trends in K_m values are offset by k_{cat} values where cephem k_{cat} is 10-fold lower than those for penams and carbapenems. As a result, all substrates examined have k_{cat}/K_m values on the order of 1×10^6 M^{-1} s^{-1}.

Demetalation of NDM. We have previously found that the colorimetric chelator 4-(2-pyridylazo)-resorcinol (PAR) removes 1 equiv of zinc from synthetic soluble dizinc NDM-1.[19,20] Incubation of PAR with folded dizinc NDM resulted in an increase in absorbance at 500 nm. Conversion of absorbance to zinc equiv by a standard curve shows that absorbance plateaus at a value equivalent to 1.0 zinc ion per protein molecule, indicating chelation of the weakly bound second zinc ion (designated Zn-2) from the active site (Figure 6A,B).[19,20,29]

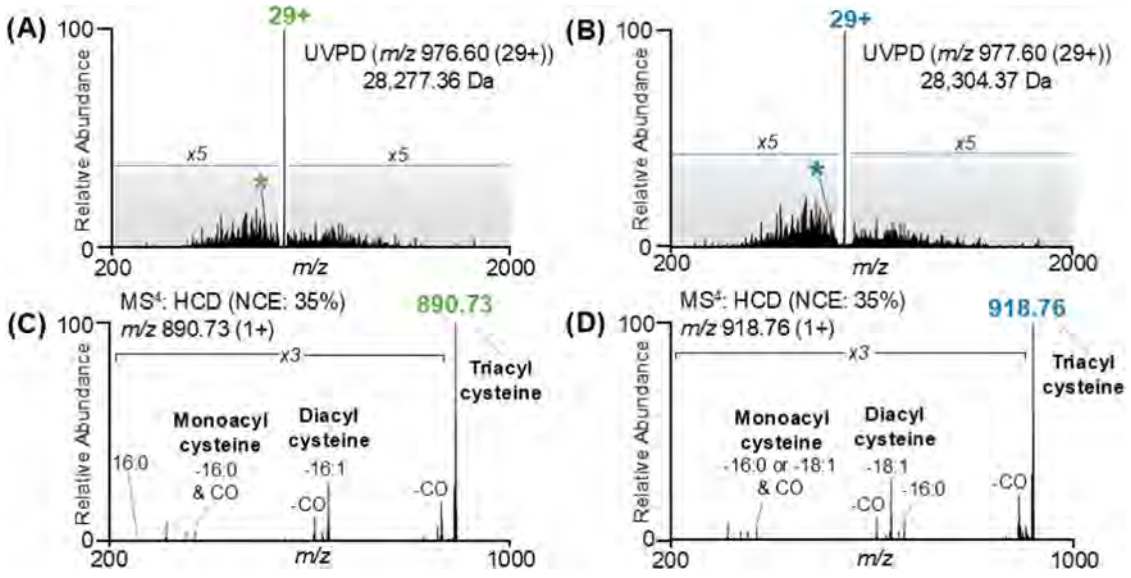

Figure 5. Top−down MS/MS analysis of Lipo-NDM-1. UVPD (1 pulse, 0.75 mJ laser energy) of Lipo-NDM-1 (29+ charge state) with masses of (A) 28,277 Da (+786 Da species) or (B) 28,305 Da (+814 Da species). The N-terminal fragment ions containing the modified cysteine are highlighted by a green or blue asterisk in panels A (m/z 890.7) and B (m/z 918.7), respectively. Based on an MS^4 method, these N-terminal fragment ions were subjected to collisional activation (HCD 35% NCE) to characterize the acyl chains of the lipid portions, confirming them as (C) C16:0/C16:1 and (D) C16:0/18:1.

https://doi.org/10.1021/acs.biochem.5c00106
Biochemistry XXXX, XXX, XXX−XXX

Table 3. Steady-State Rate Constants for Lipo-NDM-1 (Left) Compared to Soluble NDM-1 (Right) Soluble NDM-1 Values Were Determined Previously[19]

substrate	k_{cat} (s^{-1})	K_m (μMol)	k_{cat}/K_m $M^{-1}s^{-1}$	k_{cat} (s^{-1})	K_m (μ Mol)	k_{cat}/K_m M^{-1} s^{-1}
meropenem	200 ± 3	149 ± 6	1.3×10^6	138 ± 3	54 ± 3	2.6×10^6
imipenem	212 ± 10	93 ± 10	2.3×10^6	195 ± 3	45 ± 2	4.3×10^6
cephalexin	26 ± 0.8	4.4 ± 0.6	5.9×10^6	47 ± 1	5.6 ± 0.4	8.4×10^6
cefaclor	12.6 ± 0.2	2.7 ± 0.2	4.7×10^6	36 ± 1	1.8 ± 0.2	2.0×10^8
penicillin-G	302 ± 8	110 ± 13	2.7×10^6	720 ± 50	240 ± 50	3.0×10^6
ampicillin	574 ± 13	121 ± 10	4.7×10^6	690 ± 30	310 ± 30	2.2×10^6

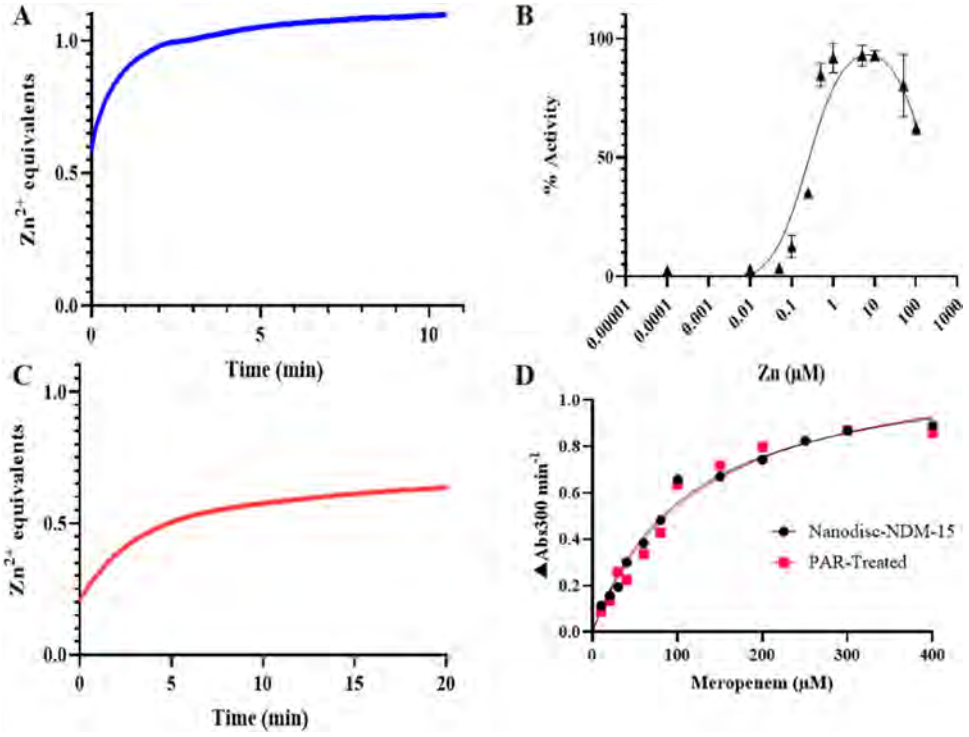

Figure 6. (A) Time-resolved chelation of dizinc Nanodisc-bound NDM-1 with 100 μM PAR. (B) Following chelation and buffer exchange, the monozinc sample is inactive until exogenous zinc is introduced. (C) Time-resolved chelation of dizinc nanodisc-bound NDM-15 with 100 μM PAR. (D) Following chelation and buffer exchange the sample displays steady-state kinetics identical to that of a dizinc sample in the absence of exogenous zinc, indicating that PAR chelation does not remove zinc from the active site.

This method is viable for the preparation of monozinc, nanodisc-bound NDM-1 as well as soluble NDM-1 and NDM-15, a clinical variant containing two mutations (M154L, A233 V) that has previously been reported to bind Zn-2 tighter than NDM-1 in soluble variants.[29] When nanodisc-bound NDM-15 is treated with PAR, the A_{500} corresponds to the Zn: PAR_n complex and does not reach a value equivalent to 1.0. Instead, the A_{500} plateaus at 0.5 equiv with subsequent change in absorbance equal to changes in background absorbance by PAR in the absence of zinc (Figure 6C). Following buffer exchange, measurement of the zinc content of the PAR-treated nanodisc-NDM-15 complex shows that the protein still binds 2 equiv of zinc. Meropenem hydrolysis rates of PAR-treated and untreated samples in the absence of exogenous zinc are nearly identical (Figure 6D), indicating that the PAR treatment method is insufficient to remove Zn-2 from lipidated NDM-15. Mono-Zn nanodisc-NDM-15 was prepared by an alternate approach in which a dizinc sample was applied to a gravity column containing the Chelex-100 resin. Following a short incubation period, the protein was eluted with a Zn-free buffer and extensively washed using centrifugal spin columns. The resultant protein sample contained 0.95−1.05 equiv of zinc. This method was only suitable for the preparation of mono-Zn nanodisc NDM-15. Chelex treatment of soluble NDM-1, soluble NDM-15, or nanodisc NDM-1 yielded overchelated samples binding less than 1 equiv of zinc (Table 4).

Characterization of Zinc Dependence. We determined that membrane anchoring impacts the binding of the second zinc ion (Zn-2) in the active site, which binds with a K_d of 1.0 μM in the soluble truncation.[29] It has been previously

Table 4. Zn Content of NDM Samples following Various Treatment Methods

sample	Zn-free purification	PAR chelation	Chelex column
soluble NDM-1	1.0	0.95−1.05	0.5−0.75
nanodisc-NDM-1	N.D.[a]	0.95−1.05	0.8
soluble NDM-15	1.4	0.95−1.05	0.8
nanodisc NDM-15	N.D.[a]	1.9−2.0	0.95−1.05

[a]N.D. not determined due to inactive/denatured protein. Purification of nanodisc-bound NDM-1 and NDM-15 in the absence of exogenous Zn resulted in extensive oxidation to Cys208, resulting in catalytically inactive protein, and was not pursued for nanodisc samples.

https://doi.org/10.1021/acs.biochem.5c00106
Biochemistry XXXX, XXX, XXX−XXX

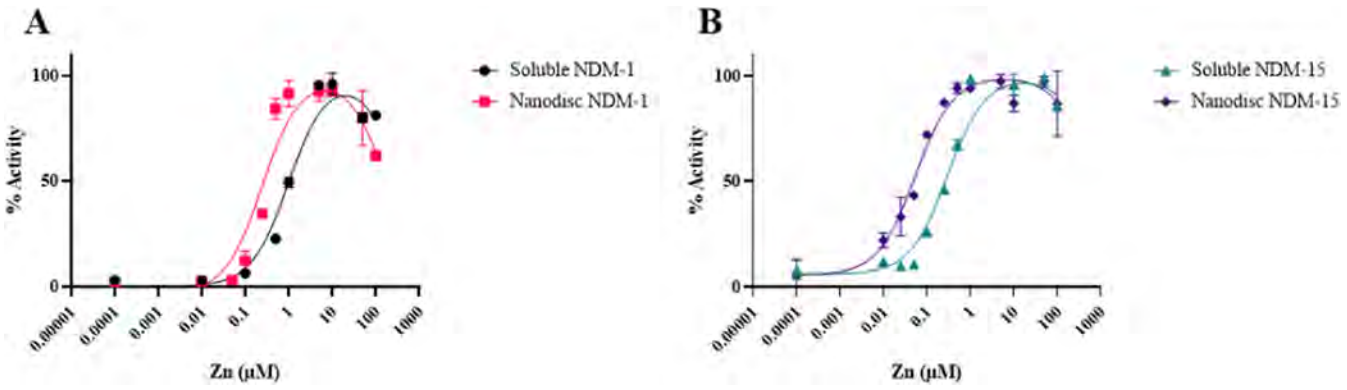

Figure 7. Zinc dependence of NDM-1 (A) and 15 (B), synthetic soluble, and nanodisc-bound proteoforms for hydrolysis of ampicillin. Rates are determined as described under experimental procedures. For each variant tested, the transition is fit as a K_d value for Zn-2 per eq 1.

demonstrated that hydrolysis of penams such as ampicillin by NDM-1 is highly sensitive to zinc concentrations and plots of this relationship have been used to determine the K_d of Zn-2 for soluble proteoforms of NDM clinical variants 1 through 17.[19,20,29] This assay was repeated to establish the K_d of Zn-2 for nanodisc-bound NDM-1 and NDM-15. The addition of increasing amounts of zinc raised activity to a maximal value, which plateaued between 1−5 μM. At higher zinc concentrations (>10 μM) a loss of activity was observed, consistent with previously observed binding to a weak third zinc-binding site.[20,41] The K_d of the stimulatory effect, representing binding to the Zn-2 site was calculated to be 250 nM for lipidated NDM-1 and 1.0 μM for the soluble variant of NDM-1 (Figure 7). Concentrations above 100 μM zinc were not examined, so an accurate fit for the K_d of Zn-3 was not determined. Previously, NDM-15 (binding 1 zinc) has been reported to display activity, with steady-state kinetic parameters that differ from the dizinc form. However, in this study, we found that mono-Zn NDM-15, both the previously studied soluble truncation and the full-length lipidated variant, display no activity in the mono-Zn form (Figure 7). We find that soluble NDM-15 binds a second Zn with a K_d of 300 nM, while the lipidated variant displays a K_d of 55 nM for Zn-2 (Table 5).

Table 5. Zn-2 Binding of NDM-1 and 15 Proteoforms

sample	Zn-2 K_d
soluble NDM-1	1.02 ± 0.16 μM
nanodisc- NDM-1	250 ± 37 nM
soluble NDM-15	300 ± 39 nM
nanodisc NDM-15	55 ± 7 nM

Membrane Binding Alters Thermostability. Nano-Differential Scanning Fluorimetry (NDSF) was used to monitor the thermal unfolding of purified NDM-1 and NDM-15 (both soluble and lipidated). Soluble NDM-1 T_m values are consistent with previously reported T_m values obtained by conventional DSF.[25,29] Lipidated NDM-1 exhibits a melting point that is 2.7 °C lower than is observed for the soluble variant (Table 6). For NDM-15 the membrane-bound proteoforms display an 8.1° increase in T_m with respect to the soluble proteoform.

Table 6. T_m Values of Soluble and Nanodisc-Bound NDM-1 and NDM-15[a]

sample	T_m (°C)
soluble NDM-1	61.3 ± 0.1
nanodisc-bound NDM-1	58.6 ± 0.1
soluble NDM-15	69.3 ± 0.1
nanodisc NDM-15	77.4 ± 0.4

[a]See Figures S6 and S7 for fluorescence plots and first derivative plots used to determine T_m.

DISCUSSION

Most studies of lipidated proteins, including BLPs, utilize detergents such as dodecylmaltoside (DDM) or (3-((3-cholamidopropyl) dimethylammonio)-1-propanesulfonate) CHAPS to solubilize proteins. Detergent solubilization of membrane proteins can lead to inactivation or poor stability often due to the loss of the native membrane environment.[47−49] In order to avoid the shortcomings of detergent solubilization and better mimic the natural environment of lipidated NDM, synthetic nanodiscs were employed to solubilize and purify NDM. Nanodiscs are 5−50 nm diameter lipid bilayer segments with a surrounding amphipathic scaffold. Conventional nanodiscs consist of a protein scaffold that stabilizes an artificially assembled lipid bilayer.[50] An evolution in nanodisc technology is the synthetic nanodisc, also referred to as a styrene-maleic acid-like lipid particle (SMALP)[51] Unlike traditional nanodiscs, synthetic nanodiscs utilize a polymer scaffold which is able to intercalate directly into native lipid membranes, extracting nanodiscs that retain the native lipid composition of the source membrane. This enables direct extraction of membrane proteins in a near-native environment.[52,53] Synthetic nanodiscs have rapidly established themselves as a powerful tool for the study of membrane-bound proteins and have seen widespread use in the biochemical characterization of integral membrane proteins from a variety of organisms.[51,54,55] In this study, we demonstrate that synthetic nanodiscs can be leveraged to study bacterial lipoproteins.

Bacterial lipoproteins are essential components of nutrient uptake and integral membrane protein insertion,[16] and in pathogenic bacteria lipoproteins are involved in host cell adhesion, virulence factor translocation, and modulation of inflammatory response.[15] Bacterial lipoproteins thus represent an appealing target for the development of new antibiotics as well as bacterial vaccines.[14,15,56] The near-native environment afforded by synthetic nanodisc purification will provide a more accurate model for the development of new antibiotics that target bacterial lipoproteins avoiding changes to conformation,

https://doi.org/10.1021/acs.biochem.5c00106
Biochemistry XXXX, XXX, XXX−XXX

stability, and ligand binding, which can be imposed by detergent solubilization.

Polymer Screening. Since synthetic nanodiscs have not been previously used to study bacterial lipoproteins, we first ascertained whether BLPs were solubilized by nanodisc-forming polymers. Fortunately, we found that lipidated NDM was readily incorporated into nanodiscs of nearly all of the tested compositions. Styrene maleic-acid (SMA) variants, the most commonly used class of nanodisc-forming polymer, were not considered for use because dicarboxylic acid motifs, such as maleic acid, inhibit metallo-β-lactamases, via nonspecific chelation of zinc (Figure 2B).[23] We first selected a variant of diisobutylenemaleic acid (DIBMA), DIBMA-glycerol, which does not contain a dicarboxylic acid motif. DIBMA-glycerol can solubilize full-length NDM-1 and showed the least impact on NDM activity when added as a free polymer, but yields did not exceed 50 μg of purified protein per liter of cell culture. To improve the yield, a library of more recently developed nanodisc-forming polymers was screened. These candidates replaced the maleic acid unit with non-chelating acrylic acid units which did not have any impact on NDM activity (Figure 2A,B).

All polymers tested during the second screen were found to solubilize lipidated NDM more effectively than DIBMA-glycerol (Figure 2C), with 6 kDa AASTY variants and CyclAPol showing the best solubilization results. Unlike widely used SMA,[57] as well as other acrylic acid-based polymers like AASTY variants, the cycloalkane units of CyclAPol are not UV absorbent, simplifying quantitation of nanodisc-bound protein and improving compatibility with UV−vis based β-lactamase activity assays. CyclAPol nanodiscs could also be stored at 4 °C for 3 weeks with no loss of activity. CyclAPol was used for all subsequent nanodisc solubilization and purification work.

Influence of Cell Culture Conditions on Lipoprotein Yield. Overexpression of lipoproteins is frequently hampered by inefficient lipid modification.[31,32] A previous study indicates that the proteoform that accumulates during overexpression is the nonlipidated preprolipoprotein, which is localized to the inner membrane and anchored by the uncleaved signal peptide (Figure 1A).[30] Indeed, visualization of the inner and outer membrane fractions following expression of NDM in a rich medium showed large amounts of NDM present in the inner membrane fraction. Only trace amounts of NDM could be detected in the outer membrane fraction by SDS-PAGE analysis, but Western Blot and β-lactamase activity assays confirmed its presence. In addition to IM-localized lipidated protein, expression in a rich medium yielded large amounts of nonmembrane-bound protein localized in the soluble lysate, consistent with previous studies of full-length NDM.[19,58] Due to poor yields from solubilizing an isolated outer membrane fraction, purification of NDM was attempted by solubilization of a total membrane sample, with the intention of separating mature triacyl-modified hololipoprotein from precursors (Figure 1A). This approach was not successful and yielded 8 mg/L of purified NDM that consisted primarily of non-nanodisc-bound soluble proteoform and trace amounts of nanodisc-bound protein. Native PAGE analysis showed soluble protein (~25 kDa) and nanodisc-lipoprotein particles (~300 kDa) (Figure 3A). Prior to solubilization, mixed membrane samples were washed extensively with high NaCl buffer to remove any residual nonmembrane-bound protein, with the final wash fraction displaying no significant β-lactamase activity. This result suggests that soluble NDM arose from the processing of previously membrane-bound protein.

Analysis of the isolated soluble proteoform by LC-MS indicated a heterogeneous mixture with molecular weights corresponding to the cleavage of N-terminal residues 16, 17, 19, and 20 (Figure 3B,C). These N-termini indicate cleavage of the full-length, unlipidated preprolipoprotein in an alanine-rich region upstream of the lipobox. Our previous work with the overexpression of full-length NDM detected soluble proteoforms with several of the same N-terminal residues as detected here,[19] suggesting a common origin between soluble protein found in the soluble lysate, and soluble protein originating from the total membrane fraction. These observations can be explained by bacterial signal peptidase I (SpI) cleavage. SpI cleaves signal peptides of periplasmic localized soluble proteins, including VIM and IMP metallo-β-lactamases recognizing an AxA motif in the signal peptide (Figure S1).[44,45]

Optimization of Expression Conditions. Accumulation of the prelipoprotein during overexpression can be alleviated by growth in an M9 minimal medium, drastically improving mature lipoprotein yield.[30] We found that growth in M9 minimal medium improved the specific yield of outer membrane-localized NDM for both NDM-1 and the clinical variant NDM-15. When grown in a rich medium, soluble lysate fractions exhibited 2-fold more β-lactamase activity than the insoluble fraction when normalized based on total protein content. Expression in M9 minimal medium inverted this result, with the insoluble fraction displaying approximately 2-fold more activity than the soluble fraction. Several alterations were made to the M9 medium based on previous reports to improve yield and reduce growth timers.[30,46] The modified medium, labeled LM9, which consistently produced the highest yield and most rapid growth rate, has an increased buffering capacity and doubles the glucose content of the standard M9 recipe (Table S2). Expression in C43(DE3) a Bl21(DE3) derivative used for the expression of toxic and integral membrane proteins,[59] was found to increase membrane localized yield approximately 2-fold compared to BL21(DE3) in LM9 medium.[30,43] As a final modification, to reduce the susceptibility of IM-localized prelipo-NDM to putative processing by SpI, we replaced the native signal peptide with a non-native lipoprotein signal peptide. We selected the signal peptide of LpP (or Braun's Lipoprotein), a structural lipoprotein that links the OM and the peptidoglycan cell wall,[60] and has been previously utilized in heterologous expression of lipoproteins in *E. coli* to improve yield.[31] The LpP-NDM chimera showed dramatically improved OM localization and was used for all subsequent purifications (Figure 4A). Incorporation of a non-native signal peptide does not alter the sequence of mature, lipidated NDM proteoform, as the sequence following the lipidated cysteine is not affected (Figures 1C and S2A). Compared with the initial conditions where NDM was frequently only detectable in the OM-enriched fraction by trace β-lactamase activity or Western blot, the final conditions produced an OM-enriched fraction in which the NDM-corresponding band on SDS-PAGE is the second most abundant protein present in the outer membrane fraction. It is likely that additional improvements can be made to optimize lipoprotein yield. Notably, the NDM-sized band in the IM-enriched fraction is of comparable size to the OM-localized band, indicating that a significant amount of protein remains in the inner membrane fraction. Potential targets for future efforts include expanded signal peptide screening and

https://doi.org/10.1021/acs.biochem.5c00106
Biochemistry XXXX, XXX, XXX−XXX

alterations to promoter strength.[31] Export via the Lol system may be another bottleneck, although overexpression of this system leads to the export of immature lipoprotein, presenting an additional challenge.[61] Nonetheless, we were able to achieve purification yields of 5−6 mg of protein per gram of solubilized OM, corresponding to roughly 1.6−2.0 mg of protein per liter of cell culture.

Significance of Soluble Proteoforms. It is unclear whether the soluble proteoforms of NDM found here and in other studies reflect a naturally occurring proteoform or an artifact of laboratory overexpression.[19,58] Sequence analysis of the NDM signal peptide does not suggest that it is optimized for SpI cleavage (Figure S2, Table S3) while Zn binding data presented here (Figure 7), and in vivo studies show lipidation imparts a significant fitness advantage.[13,28] This advantage is particularly apparent under Zn limiting conditions which are proposed to be the primary force driving metallo-carbapenemase evolution.[62,63] The soluble proteoforms detected here may thus simply be an artifact of heterologous overexpression, which has been shown to result in accumulation of inner membrane localized prelipoprotein species.[30] These accumulated species may be susceptible to off-target processing by SpI due to the alanine-rich region found in the NDM signal peptide. Off-target activity by SpI of a poorly optimized substrate may also explain the nonhomogeneous cleavage pattern of soluble proteoforms, where the calculated N-termini of the soluble proteoforms align to an alanine-rich region, only proteoform D, (Figure 3C) aligns to a canonical SpI recognition site with alanine at the −1 and −3 site, though SpI is able to accept a variety of small polar residues at −1 and −3 sites.[44,45] Additional studies that characterize proteoform ratios following expression driven by the native promoter found in the $_{bla}$NDM gene may be needed to further probe the biological relevance and origin of soluble NDM proteoforms.

Nanodisc Characterization. Light scattering analysis of purified NDM-CyclAPol nanodiscs shows a monodisperse species with an estimated molecular weight of 311 kDa, consistent with what is estimated from native PAGE with molecular weight standards. DLS analysis indicates that the NDM-containing nanodiscs have a diameter of 40.8 nm. Synthetic nanodisc diameters range from 5 to 60 nm and are highly variable and dependent on polymer: membrane ratios, membrane composition, and solubilization conditions.[49] Particularly, the impact of the unique lipid composition of the Gram-negative outer membrane on nanodisc size remains unexplored.

Mass Spectrometry. The nanodisc-bound fraction of NDM-1 was analyzed by mass spectrometry (MS) to determine the molecular weight of lipidated NDM-1 (Figure S4). MS was previously used to study lipidated NDM-1 using collisional activation,[64] a similar approach was used in the current study involving UVPD. Two major proteoforms (28277 and 28304 Da) were measured (Figure 5), and each proteoform was subjected to ultraviolet photodissociation (UVPD) and proton transfer charge reduction (PTCR) to characterize the primary sequence features of the lipidated NDM-1 species. UVPD provided extensive sequence coverage of both proteoforms (67% for the C16:0/C16:1 and 64% for the C16:0/18:1 species, respectively) (Figure S5), including fragment ions originating from cleavage adjacent to the N-terminal cysteine for each proteoform. These fragment ions containing the cysteine residue (bearing a mass shift of +786 or +814 Da) were isolated and subjected to collisional activation (via HCD), providing insight into the identities of the acyl chains attached to the N-terminal cysteine of each proteoform.[63] The molecular weights of the acyl chains identified by this multistage UVPD/PTCR/HCD approach are consistent with modification by a mixture of C16 and C18 saturated/monounsaturated lipids, the most widely observed lipids found in bacterial lipoproteins.[16] The acyl chains appended to bacterial lipoproteins are ultimately derived from inner membrane phospholipids, as such the lipid identity of BLPs is reflective of the inner membrane lipid composition.[65]

Enzyme Characterization. Comparison of the steady-state kinetic parameters of nanodisc-bound NDM-1 with existing data for soluble NDM-1 indicates that membrane binding has minimal effects on β-lactam hydrolysis. Lipidated NDM retains the broad substrate profile that is typical of metallo-carbapenemases, processing β-lactams of the three most widely used classes (penams, cephems, and carbapenems) (Table 3). Compared with the soluble construct, lipidated NDM-1 displays less difference in activity between penams (penicillin-G and ampicillin) and carbapenems (meropenem, imipenem). The K_m and k_{cat} values are an order of magnitude lower for cephems (cephalexin, cefaclor) although the reported k_{cat}/K_m values are on the order of 10^6 M^{-1} s^{-1} unlike the 10^7 M^{-1} s^{-1} values reported for soluble NDM-1. Different active site interactions are involved in the binding of each β-lactam class, minor structural perturbations or changes in protein flexibility may account for differences in kinetic parameters between lipidated and soluble NDM-1 which differ by substrate class.[66]

In vivo studies of full-length NDM have suggested that membrane binding improves enzyme stability under zinc starvation conditions. Studies comparing NDM with related MBLs indicate that lipidated NDM displays improved stability *in vivo* compared with VIM, IMP, and synthetic soluble NDM proteoforms, including in the presence of calprotectin, a neutrophil secreted chelating protein involved in nutritional immunity.[13,33] Similarly, *in vitro* characterization of NDM variants 1−17 demonstrates a progressive increase in Zn affinity, indicating that Zn affinity is the primary factor driving the evolution of NDM.[62,67] Measurements of MBL Zn affinity values are complicated by differences in conditions and techniques across studies, which even results in uncertainty of the mode of Zn binding.[68−70] and the potential for facile movement of metal ions between the Zn-1 and Zn-2 binding sites in mono-Zn species,[71] although this has not been demonstrated in NDM, we cannot unequivocally rule out the presence of NDM species other than the putative mono-Zn species with Zn at the Zn-1 site. Comparison of Zn affinity in this study is thus limited only to other data collected using this same technique.[29] We find that purified lipidated NDM-1 binds Zn-2 4x tighter, with a K_d of 250 nM compared to 1.0 μM for the soluble construct. For NDM-15, a similar relationship is observed, with lipidated NDM-15 binding Zn-2 with a K_d of 55 nM compared to 300 nM for the soluble variant (Table 5).[13,27] These results support the hypothesis that selective pressure for activity and stability at low Zn concentrations is the primary factor driving the evolution of NDM clinical variants.

Despite the observed improvement in zinc affinity, lipidated NDM-1 exhibits reduced thermostability compared with synthetic soluble truncation. Lipidated NDM-1 displays a T_m of 58.6 ± 0.1 compared with 61.3 ± 0.1 for the soluble construct. In contrast, lipidated NDM-15 displays increased

https://doi.org/10.1021/acs.biochem.5c00106
Biochemistry XXXX, XXX, XXX−XXX

thermostability vs the soluble construct, with a Tm of 77.4 ± 0.4, 8° higher than soluble NDM-15 (Table 6). The T_m we report for soluble NDM-1 is several degrees higher than has been previously reported, while the T_m we report for nanodisc NDM is comparable with previously reported soluble values.[29,72] Thermostability may not properly capture the impact of lipidation, which has been shown to improve protein half-life in vivo as well as resistance to proteolytic degradation following demetalation in vivo.[13,27] A possible mechanism behind both the improved Zn affinity reported in this study and improved stability reported in vivo is a proposed network of electrostatic interactions between surface exposed residues of NDM and the phosphate head groups of the lipid surface play a role in orienting and stabilizing lipidated NDM.[27,28] Future studies will further elucidate these electrostatic interactions.

Comparison of NDM-1 and NDM-15. It has been proposed that in addition to evolution for improved Zn binding, NDM clinical variants have gained function as mono-Zn enzymes with NDM-15 having the highest mono-Zn activity.[29] Monozinc MBLs are not unknown, B2 MBLs like CphA are definitionally mono-Zn enzymes.[73,74] However, B2 MBLs display key differences from B1MBLs like NDM with regard to substrate profile, Zn coordination, and active site conformation.[75−77] Unlike the previous characterization of NDM-15, we find no evidence that NDM-15 is active as a monozinc enzyme (Figure 7). Monozinc samples of NDM-15, both soluble and nanodisc-bound, display only trace activity prior to zinc supplementation. Previous work on soluble NDM-15 was conducted using a process that was demonstrated to produce mono-Zn sample of soluble NDM-1(Table 4).[19,29] However, the putative mono-Zn NDM-15 sample was not measured for the Zn content prior to analysis. Repeating this method, we found that the soluble NDM-15 sample contained 1.4−1.6 equiv of Zn. Using our newly developed mono-Zn preparation methods of continuously monitored PAR chelation (for soluble NDM-15) or Chelex treatment (for nanodisc NDM-15), we isolated NDM-15 samples that contain between 0.95 and 1.05 equiv of zinc. These samples, in the absence of exogenous Zn, show only trace activity that can easily be explained by ∼ 5% of the sample still being in the di-Zn form. Future studies probing the characteristics of mono-Zn NDM may incorporate EPR spectroscopy to further characterize the active site of the inactive mono-Zn form.[29] We propose that NDM-15 is not active as a mono-Zn enzyme but is a canonical B1 MBL that has evolved a higher affinity for Zn-2 compared to other NDM variants, with a reported Zn-2 K_d of 300 nM for the soluble variant and 55 nM for the nanodisc-bound variant (Figure 7).

CONCLUSIONS

Our biochemical characterization of nanodisc-bound lipidated NDM is consistent with the hypothesis that lipidation and membrane anchoring improves fitness under zinc-limiting conditions, representing an adaptation to the conditions imposed by nutritional immunity during infection.[20,33,34] We found improvement in Zn binding imparted by lipidation enhances the affinity for the crucial Zn-2 ion 4-fold in NDM-1 and 6-fold in NDM-15, which contains the most widely conserved mutations found in NDM clinical variants. We also found that NDM-15 is active only in the di-Zn form, consistent with its classification as a canonical B1 metallo-β-lactamase. Lipidation has a less consistent impact on thermostability, with lipidated NDM-1 displaying moderately reduced thermostability compared to that of soluble truncation. In NDM-15, lipidation is found to improve thermostability by 8 degrees. Lipidation has previously been shown to improve stability *in vivo* by improved resistance to proteolytic degradation, indicating that thermostability may not fully model the impacts of lipidation on stability. Future studies will leverage the retention of the native membrane environment afforded by synthetic nanodiscs to probe the impact of lipidation on stability of the mono-Zn proteoform and the potential role that proposed electrostatic interactions between the anionic phosphate head groups of outer membrane lipids and positively charged residues in the globular region of NDM. The role of these proposed electrostatic interactions in stabilizing both the active dizinc form and the inactive monozinc form will be probed.

NDM is the only known lipidated MBL found in pathogenic bacteria, but it is likely not unique among the MBLs. Metagenomics analysis suggests that numerous putative lipidated MBLs are present in soil microbes.[13] A BLAST search of the NCBI protein databank using NDM-1 (NCBI Protein database Accession # CAZ39946) returns 293 uncharacterized MBLs which are predicted to be lipidated by SignalP.[78] A substantial reservoir of novel lipidated MBLs likely exists. Of note is the recently described *Alcaligenes faecalis*-derived MBL (AFM).[79,80] Though not characterized in existing studies, AFM contains a predicted lipidation signal peptide (Figure S2, Table S3). AFM displays high sequence identity (85%) with NDM-1, rising to 90% after cleavage at the predicted lipobox, by comparison, VIM and IMP have a maximum of 32% sequence identity with NDM. Point mutations found in NDM clinical variants are also observed in all AFM variants, (Figure S8), indicating a possible recent origin from NDM. In addition to metallo-β-lactamases a recent study indicates that lipidation is widespread in class-D Serine-β-lactamases, with 60% Class-D enzymes variants including clinically relevant carbapenem hydrolyzing Oxacillinase (OXA) variants being identified as lipoproteins.[81] The emergence of new lipidated β-lactamases in the clinic, along with the existence of hundreds of uncharacterized putative lipidated MBLs highlights the need for continued study of the functional impact of lipidation on metallo-β-lactamase activity to account for evolutionary trends in antibiotic resistance and ensure informed development of future β-lactamase inhibitors. This work provides the foundation for these studies as well as a workflow for the use of synthetic nanodiscs to study other bacterial lipoproteins.

ASSOCIATED CONTENT

Supporting Information

The Supporting Information is available free of charge at https://pubs.acs.org/doi/10.1021/acs.biochem.5c00106.

Substrate difference extinction coefficients, Diagram of signal peptide cleavage by signal peptidase I (SpI), Composition of minimal media, graphical output of predicted signal peptide cleavage patterns using SignalP 6.0 for NDM-1, LpP, LpP-NDM-1 chimera, IMP-1, AFM-1, and VIM-2, numerical output of predicted signal peptide cleavage patterns using SignalP 6.0 for NDM-1, LpP, LpP-NDM-1 chimera, IMP-1, AFM-1, and VIM-2, purification of LpP-NDM-1 chimera in CyclApol nanodiscs, ESI mass spectra of lipidated NDM-1,

https://doi.org/10.1021/acs.biochem.5c00106
Biochemistry XXXX, XXX, XXX−XXX

sequence coverage of lipidated NDM-1 by UVPD/PTCR, first derivative plots of fluorescence ratios at 350 and 330 nm for soluble and nanodisc-bound NDM-1 and NDM-15, temperature resolved fluorescence traces at 350 and 330 nm for soluble and nanodisc-bound NDM-1 and NDM-15, sequence alignments of NDM-1, NDM-14, NDM-24, AFM1-5, IMP-1, and VIM-2, NCBI accession codes for NDM-1, NDM-14, NDM-24, AFM1-5, IMP-1, and VIM-2 (PDF)

AUTHOR INFORMATION

Corresponding Author

Christian P. Whitman − *Division of Chemical Biology and Medicinal Chemistry, College of Pharmacy, University of Texas at Austin, Austin, Texas 78712, United States;* orcid.org/0000-0002-8231-2483; Phone: (512) 471-6198; Email: whitman@austin.utexas.edu; Fax: (512) 232-2606

Authors

Thomas Smisek − *Department of Molecular Biosciences, The University of Texas at Austin, Austin, Texas 78712, United States;* orcid.org/0009-0007-4085-1976

Nemanja Vuksanovic − *Department of Chemistry, Boston University, Boston, Massachusetts 02215, United States;* orcid.org/0000-0003-2883-6312

Jada N. Walker − *Department of Chemistry, The University of Texas at Austin, Austin, Texas 78712, United States;* orcid.org/0000-0001-6233-3124

Haily Vu − *Department of Molecular Biosciences, The University of Texas at Austin, Austin, Texas 78712, United States*

Dann D. Rivera − *Division of Chemical Biology and Medicinal Chemistry, College of Pharmacy, University of Texas at Austin, Austin, Texas 78712, United States*

[⊥]**Walter Fast** − *Division of Chemical Biology and Medicinal Chemistry, College of Pharmacy, University of Texas at Austin, Austin, Texas 78712, United States;* orcid.org/0000-0001-7567-2213

Jennifer S. Brodbelt − *Department of Chemistry, The University of Texas at Austin, Austin, Texas 78712, United States;* orcid.org/0000-0003-3207-0217

Complete contact information is available at: https://pubs.acs.org/10.1021/acs.biochem.5c00106

Funding

This research was supported by the Robert A. Welch Foundation (Grants F-2125 to C.P.W., F-1155 to J.S.B.) and the National Science Foundation (CHE2203602 to J.S.B.) and the National Institutes of Health Grant F32 GM146421 to N.V.

Notes

The authors declare no competing financial interest.

[⊥]Deceased December 4, 2023.

ACKNOWLEDGMENTS

The authors dedicate this paper to the memory of our cherished colleague Professor Walter Fast. The authors thank Prof. Michael Crowder (Miami University of Ohio, Oxford, OH) for helpful discussions and Dr. Tamer Kaoud for technical help with the dynamic light scattering experiments. Figures were generated using BioRender.com. Soluble protein digestion and protein molecular weight analysis were performed by Peter Faull and Andrew Basalla, respectively, at the UT Austin Center for Biomedical Research Support Biological Mass Spectrometry Facility (RRID:SCR_021728).

ABBREVIATIONS

AASTY, acrylic acid costyrene; $_{bla}$NDM, New Delhi metallo-β-lactamase; BLP, bacterial lipoprotein; CHAPS, (3-((3-cholamidopropyl)dimethylammonio)-1-propanesulfonate); DDM, dodecylmaltoside; DIBMA, diisobutylenemaleic acid; DLS, dynamic light scattering; IMP, imipenemase; IM, inner membrane; KPC, *Klebsiella pneumoniae* carbapenemase; Lgt, lipoprotein diacyl glyceryl transferase; LM9, lipoprotein M9 minimal media; Lnt, lipoprotein N-acyl transferase; Lol, lipoprotein outer membrane localization; LC-MS, liquid chromatography−mass spectrometry; LB, Lysogeny broth; MBL, metallo-β-lactamases; MWCO, molecular weight cutoff; NDM, New Delhi metallo-β-lactamase; NDSF, nanodifferential scanning fluorimetry; OXA-48, oxacillinase-48-like carbapenemase; IM, inner membrane; OM, outer membrane; PAR, 4-(2-pyridylazo)-resorcinol; SpI, signal peptidase-I; SDS-PAGE, sodium dodecyl sulfate-polyacrylamide gel electrophoresis; SMALP, styrene-maleic acid-like lipid particles; VIM, Verona integron-encoded metallo-β-lactamase

REFERENCES

(1) Bush, K.; Bradford, P. A. Bush and Bradford - 2016 - β-Lactams and β-Lactamase Inhibitors An Overview.pdf. *Cold Spring Harbor Perspect. Med.* **2016**, *22*, No. a025247, DOI: 10.1101/cshperspect.a025247.

(2) Bush, K. Past and present perspectives on β-lactamases. *Antimicrob. Agents Chemother.* **2018**, *62*, No. e01076-18.

(3) Bush, K.; Bradford, P. A. Epidemiology of β-Lactamase-Producing Pathogens. *Clin. Microbiol. Rev.* **2020**, *33*, No. e00047-19.

(4) Boutzoukas, A. E.; Komarow, L.; Chen, L.; Hanson, B.; Kanj, S. S.; Liu, Z.; Salcedo Mendoza, S.; Ordoñez, K.; Wang, M.; Paterson, D. L.; Evans, S.; Ge, L.; Giri, A.; Hill, C.; Baum, K.; Bonomo, R. A.; Kreiswirth, B.; Patel, R.; Arias, C. A.; Chambers, H. F.; Fowler, V. G.; van Duin, D.; Investigators, M.-D. R. O. N.; Souha, S. K.; Jean, F. (Jeff) J.; Fujie, Z.; Judith, J. L.; Robert, A. S.; Martin, S.; Valentina, D. C.; Jose, M. O. G.; Eric, C.; Susan, R.; Deverick, J. A.; Beth, E.; Carol, H.; Heather, R. C.; Keri, B.; Rebekka, A.; Vance, G. F.; Karen, O.; Jesse, T. J.; Linghua, L.; Barry, N. K.; Claudia, M.; Liang, C.; Samit, D.; Erica, H.; Ezequiel, C.; Maria, R.; Samuel, V.; Marisa, L. S.; Sandra, V.; Jairo, F.; Cesar, A. A.; An, Q. D.; Diane, P.; Kirsten, R.; Truc, T. T.; Fupin, H.; Jiachun, S.; Jianping, J.; Minggui, W.; Xiaogang, X.; Yang, Y.; Jose, M. M.; Maria, S.; Thamer, A.; Robert, A. B.; Steven, H. M.; Susan, D. R.; Charles, H.; Kerry, G.-Q.; Robin, P.; Suzannah, S.-M.; Sara, R.; Glenn, W.; Robert, C. K.; Greg, W.; Belinda, O.; Gopi, P.; Daniel, E.; Angela, K.; Julia, G.-D.; Soraya, S.; John, J. F.; Zhengyin, L.; Andrew, H.; David, L. P.; Qing, X.; Keith, S. K.; Hainv, G.; Yunsong, Y.; Mary, W.; Bettina, C. F.; Brandon, E.; Kalisvar, M.; Kean, L. C.; Nares, S.; Paul, A. T.; Jason, C. G.; Anton, P.; Marcel, L.; Lanjuan, L.; Lauren, K.; Lizhao, G.; Scott, E.; Todd, M.; Henry, F. C.; Omai, B. G.; Lilian, M. A.; David, van D.; Ebbing, L.; Jennifer, H. H.; Yohei, D.; Darren, W.; Blake, H.; Jinnethe, R.; Maria, V. V. B.; Lorena, D.; Federico, P.; Ritu, B.; Sorabh, D.; Michael, J. S.; Zhiyong, Z. International Epidemiology of Carbapenemase-Producing *Escherichia coli*. *Clin. Infect. Dis.* **2023**, *77*, 499−509.

(5) Kohler, P. P.; Melano, R. G.; Patel, S. N.; Shafinaz, S.; Faheem, A.; Coleman, B. L.; Green, K.; Armstrong, I.; Almohri, H.; Borgia, S.; Borgundvaag, E.; Johnstone, J.; Katz, K.; Lam, F.; Muller, M. P.; Powis, J.; Poutanen, S. M.; Richardson, D.; Rebbapragada, A.; Sarabia, A.; Simor, A. Emergence of Carbapenemase- Producing Enter-

obacteriaceae, South-Central Ontario, Canada. *Emerging Infect. Dis.* **2018**, *24*, 1674−1682.
(6) Wagenlehner, F. M.; Gasink, L. B.; McGovern, P. C.; Moeck, G.; McLeroth, P.; Dorr, M.; Dane, A.; Henkel, T. Cefepime−Taniborbactam in Complicated Urinary Tract Infection. *N. Engl. J. Med.* **2024**, *390*, 611−622.
(7) Zalacain, M.; Lozano, C.; Llanos, A.; Sprynski, N.; Valmont, T.; de Piano, C.; Davies, D.; Leiris, S.; Sable, C.; Ledoux, A.; Morrissey, I.; Lemonnier, M.; Everett, M. Novel Specific Metallo-β-Lactamase Inhibitor ANT2681 Restores Meropenem Activity to Clinically Effective Levels against NDM-Positive Enterobacterales. *Antimicrob. Agents Chemother.* **2021**, *65*, No. e00203−21.
(8) Griffith, D.; Roberts, J.; Wallis, S.; Hernandez-Mitre, M. P.; Morgan, E.; Gehrke, S.; Dudley, M.; Loutit, J. 216. A Phase 1 Study of the Safety, Tolerability, and Pharmacokinetics of Multiple Doses of the Beta-lactamase inhibitor Xeruborbactam Alone and in Combination Meropenem in Healthy Adult Subjects. *Open Forum Infect. Dis.* **2022**, *9*, No. ofac492.294.
(9) Dong, H.; Li, Y.; Cheng, J.; Xia, Z.; Liu, W.; Yan, T.; Chen, F.; Wang, Z.; Li, R.; Shi, J.; Qin, S.; Martin, R. M. Genomic Epidemiology Insights on NDM-Producing Pathogens Revealed the Pivotal Role of Plasmids on blaNDM Transmission. *Microbiol. Spectrum* **2022**, *10*, No. e02156-21.
(10) Khan, A. U.; Maryam, L.; Zarrilli, R. Structure, Genetics and Worldwide Spread of New Delhi Metallo-β-lactamase (NDM): a threat to public health. *BMC Microbiol.* **2017**, *17*, No. 101.
(11) Carbapenem-Resistant Enterobacterales | A.R. & Patient Safety Portal.
(12) King, D.; Strynadka, N. Crystal structure of New Delhi metallo-β-lactamase reveals molecular basis for antibiotic resistance. *Protein Sci.* **2011**, *20*, 1484−1491.
(13) González, L. J.; Bahr, G.; Nakashige, T. G.; Nolan, E. M.; Bonomo, R. A.; Vila, A. J. Membrane anchoring stabilizes and favors secretion of New Delhi metallo-β-lactamase. *Nat. Chem. Biol.* **2016**, *12*, 516−522.
(14) Smithers, L.; Olatunji, S.; Caffrey, M. Bacterial Lipoprotein Posttranslational Modifications. New Insights and Opportunities for Antibiotic and Vaccine Development. *Front. Microbiol.* **2021**, *12*, No. 3802.
(15) Kovacs-Simon, A.; Titball, R. W.; Michell, S. L. Lipoproteins of bacterial pathogens. *Infect. Immun.* **2011**, *79*, 548−561.
(16) Nakayama, H.; Kurokawa, K.; Lee, B. L. Lipoproteins in bacteria: Structures and biosynthetic pathways. *FEBS J.* **2012**, *279*, 4247−4268.
(17) Zückert, W. R. Secretion of Bacterial Lipoproteins: Through the Cytoplasmic Membrane, the Periplasm and Beyond. *Biochim. Biophys. Acta, Mol. Cell Res.* **2014**, *1843*, 1509−1516.
(18) Narita, S. I.; Matsuyama, S. I.; Tokuda, H. Lipoprotein trafficking in *Escherichia coli*. *Arch. Microbiol.* **2004**, *182*, 1−6.
(19) Thomas, P. W.; Zheng, M.; Wu, S.; Guo, H.; Liu, D.; Xu, D.; Fast, W. Characterization of Purified New Delhi Metallo-β-lactamase-1. *Biochemistry* **2011**, *50*, 10102−10113.
(20) Stewart, A. C.; Bethel, C. R.; Vanpelt, J.; Bergstrom, A.; Cheng, Z.; Miller, C. G.; Williams, C.; Poth, R.; Morris, M.; Lahey, O.; Nix, J. C.; Tierney, D. L.; Page, R. C.; Crowder, M. W.; Bonomo, R. A.; Fast, W. Clinical Variants of New Delhi Metallo-β-Lactamase Are Evolving to Overcome Zinc Scarcity. *ACS Infect. Dis.* **2017**, *3*, 927−940.
(21) King, D. T.; Worrall, L. J.; Gruninger, R.; Strynadka, N. New delhi metallo-β-lactamase: Structural insights into β-lactam recognition and inhibition. *J. Am. Chem. Soc.* **2012**, *134*, 11362−11365.
(22) Saini, A.; Bansal, R. Insights on the structural characteristics of NDM-1: The journey so far. *Adv. Biol. Chem.* **2012**, *02*, 323−334.
(23) Chen, A. Y.; Thomas, P. W.; Stewart, A. C.; Bergstrom, A.; Cheng, Z.; Miller, C.; Bethel, C. R.; Marshall, S. H.; Credille, C. V.; Christopher, L.; Page, R. C.; Bonomo, R. A.; Crowder, M. W.; Tierney, D. L.; Fast, W.; Cohen, S. M. Dipicolinic Acid Derivatives as Inhibitors of New Delhi Metallo-β- lactamase-1. *J. Med. Chem* **2018**, *60*, 7267−7283.
(24) Krajnc, A.; Brem, J.; Hinchliffe, P.; Calvopiña, K.; Panduwawala, T. D.; Lang, P. A.; Kamps, J. J. A. G.; Tyrrell, J. M.; Widlake, E.; Saward, B. G.; Walsh, T. R.; Spencer, J.; Schofield, C. J. Bicyclic Boronate VNRX-5133 Inhibits Metallo- And Serine-β-Lactamases. *J. Med. Chem.* **2019**, *62*, 8544−8556.
(25) Thomas, P. W.; Cho, E. J.; Bethel, C. R.; Smisek, T.; Ahn, Y.-C.; Schroeder, J. M.; Thomas, C. A.; Dalby, K. N.; Beckham, J. T.; Crowder, M. W.; Bonomo, R. A.; Fast, W. Discovery of an Effective Small-Molecule Allosteric Inhibitor of New Delhi Metallo-β-lactamase (NDM). *ACS Infect. Dis.* **2022**, *8*, 811−824.
(26) Gonzalez, L. J.; Bahr, G.; Vila, A. J. Lipidated β-lactamases: from bench to bedside. *Future Microbiol.* **2016**, *11*, 1495−1498, DOI: 10.2217/fmb-2016-0176.
(27) González, L. J.; Bahr, G.; González, M. M.; Bonomo, R. A.; Vila, A. J. In-cell kinetic stability is an essential trait in metallo-β-lactamase evolution. *Nat. Chem. Biol.* **2023**, *19*, 1116−1126.
(28) Prunotto, A.; Bahr, G.; González, L. J.; Vila, A. J.; Dal Peraro, M.; Peraro, M. D.; Dal Peraro, M. Molecular Bases of the Membrane Association Mechanism Potentiating Antibiotic Resistance by New Delhi Metallo-β-lactamase 1. *ACS Infect. Dis.* **2020**, *6*, 2719−2731.
(29) Cheng, Z.; Thomas, P. W.; Ju, L.; Bergstrom, A.; Mason, K.; Clayton, D.; Miller, C.; Bethel, C. R.; VanPelt, J.; Tierney, D. L.; Page, R. C.; Bonomo, R. A.; Fast, W.; Crowder, M. W. Evolution of New Delhi metallo-β-lactamase (NDM) in the clinic: Effects of NDM mutations on stability, zinc affinity, and mono-zinc activity. *J. Biol. Chem.* **2018**, *293*, 12606−12618.
(30) Tseng, C. L.; Leng, C. H. Influence of medium components on the expression of recombinant lipoproteins in *Escherichia coli*. *Appl. Microbiol. Biotechnol.* **2012**, *93*, 1539−1552.
(31) Hansson, L.; Noppa, L.; Nilsson, A. K.; Strömqvist, M.; Bergström, S. Expression of Truncated and Full-Length Forms of the Lyme Disease Borrelia Outer Surface Protein A in *Escherichia coli*. *Protein Expression Purif.* **1995**, *6*, 15−24.
(32) Babu, M. M.; Priya, M. L.; Selvan, A. T.; Madera, M.; Gough, J.; Aravind, L.; Sankaran, K. A database of bacterial lipoproteins (DOLOP) with functional assignments to predicted lipoproteins. *J. Bacteriol.* **2006**, *188*, 2761−2773.
(33) Zygiel, E. M.; Nolan, E. M. Transition Metal Sequestration by the Host-Defense Protein Calprotectin. *Annu. Rev. Biochem.* **2018**, *87*, 621−643.
(34) CLOHESSY, P. A.; GOLDEN, B. E. Calprotectin-Mediated Zinc Chelation as a Biostatic Mechanism in Host Defence. *Scand. J. Immunol.* **1995**, *42*, 551−556.
(35) Yu, S.; Vosbeek, A.; Corbella, K.; Severson, J.; Schesser, J.; Sutton, L. D. A chromogenic cephalosporin for β-lactamase inhibitor screening assays. *Anal. Biochem.* **2012**, *428*, 96−98.
(36) Cian, M. B.; Giordano, N. P.; Mettlach, J. A.; Minor, K. E.; Dalebroux, Z. D. Separation of the Cell Envelope for Gram-negative Bacteria into Inner and Outer Membrane Fractions with Technical Adjustments for Acinetobacter baumannii *J. Visualized Exp.* 2020, DOI: 10.3791/60517.
(37) Oluwole, A. O.; Danielczak, B.; Meister, A.; Babalola, J. O.; Vargas, C.; Keller, S. Solubilization of Membrane Proteins into Functional Lipid-Bilayer Nanodiscs Using a Diisobutylene/Maleic Acid Copolymer. *Angew. Chem., Int. Ed.* **2017**, *56*, 1919−1924.
(38) Pollock, N. L.; Rai, M.; Simon, K. S.; Hesketh, S. J.; Teo, A. C. K.; Parmar, M.; Sridhar, P.; Collins, R.; Lee, S. C.; Stroud, Z. N.; Bakker, S. E.; Muench, S. P.; Barton, C. H.; Hurlbut, G.; Roper, D. I.; Smith, C. J. I.; Knowles, T. J.; Spickett, C. M.; East, J. M.; Postis, V. L. G.; Dafforn, T. R. SMA-PAGE: A new method to examine complexes of membrane proteins using SMALP nano-encapsulation and native gel electrophoresis. *Biochim. Biophys. Acta, Biomembr.* **2019**, *1861*, 1437−1445.
(39) Juetten, K. J.; Brodbelt, J. S. MS-TAFI: A Tool for the Analysis of Fragment Ions Generated from Intact Proteins. *J. Proteome Res.* **2023**, *22*, 546−550.
(40) Melkonian, T. R.; Vuksanovic, N.; Person, M. D.; Chen, T.-Y.; Chang, W.; Allen, K. N.; Whitman, C. P. Beyond the $\beta-\alpha-\beta$ Fold: Characterization of a SnoaL Domain in the Tautomerase Superfamily.

https://doi.org/10.1021/acs.biochem.5c00106
Biochemistry XXXX, XXX, XXX−XXX

Biochemistry **2025**, *64* (9), 1950−1962, DOI: 10.1021/acs.biochem.5c00051.
(41) Stewart, A. *An Investigation of New Delhi metallo-[beta]-lactamase: Clinical Variants, Lipid Modification & Inhibition*; The University of Texas at Austin: Austin, TX, 2017.
(42) Beis, K.; Whitfield, C.; Booth, I.; Naismith, J. H. Two-step purification of outer membrane proteins. *Int. J. Biol. Macromol.* **2006**, *39*, 10−14.
(43) Filip, C.; Fletcher, G.; Wulff, J. L.; Earhart, C. F. Solubilization of the cytoplasmic membrane of *Escherichia coli* by the ionic detergent sodium-lauryl sarcosinate. *J. Bacteriol.* **1973**, *115*, 717−722.
(44) Auclair, S. M.; Bhanu, M. K.; Kendall, D. A. Signal peptidase I: Cleaving the way to mature proteins. *Protein Sci.* **2012**, *21*, 13−25.
(45) Paetzel, M. Structure and mechanism of *Escherichia coli* type I signal peptidase. *Biochim. Biophys. Acta, Mol. Cell Res.* **2014**, *1843*, 1497−1508.
(46) Azatian, S. B.; Kaur, N.; Latham, M. P. Increasing the buffering capacity of minimal media leads to higher protein yield. *J. Biomol. NMR* **2019**, *73*, 11.
(47) Seddon, A. M.; Curnow, P.; Booth, P. J. Membrane proteins, lipids and detergents: not just a soap opera. *Biochim. Biophys. Acta, Biomembr.* **2004**, *1666*, 105−117.
(48) Yang, Z.; Wang, C.; Zhou, Q.; An, J.; Hildebrandt, E.; Aleksandrov, L. A.; Kappes, J. C.; DeLucas, L. J.; Riordan, J. R.; Urbatsch, I. L.; Hunt, J. F.; Brouillette, C. G. Membrane protein stability can be compromised by detergent interactions with the extramembranous soluble domains. *Protein Sci.* **2014**, *23*, 769.
(49) Krishnarjuna, B.; Ramamoorthy, A. Detergent-Free Isolation of Membrane Proteins and Strategies to Study Them in a Near-Native Membrane Environment. 2022.
(50) Hagn, F.; Etzkorn, M.; Raschle, T.; Wagner, G. Optimized phospholipid bilayer nanodiscs facilitate high-resolution structure determination of membrane proteins. *J. Am. Chem. Soc.* **2013**, *135*, 1919−1925.
(51) Ayub, H.; Clare, M.; Milic, I.; Chmel, N. P.; Böning, H.; Devitt, A.; Krey, T.; Bill, R. M.; Rothnie, A. J. CD81 extracted in SMALP nanodiscs comprises two distinct protein populations within a lipid environment enriched with negatively charged headgroups. *Biochim. Biophys. Acta, Biomembr.* **2020**, *1862*, No. 183419.
(52) Dörr, J. M.; Koorengevel, M. C.; Schäfer, M.; Prokofyev, A. V.; Scheidelaar, S.; Van Der Cruijsen, E. A. W.; Dafforn, T. R.; Baldus, M.; Killian, J. A. Detergent-free isolation, characterization, and functional reconstitution of a tetrameric K + channel: The power of native nanodiscs *PNAS 111* 5218607 18612 DOI: 10.1073/pnas.1416205112.
(53) Scheidelaar, S.; Koorengevel, M. C.; Pardo, J. D.; Meeldijk, J. D.; Breukink, E.; Killian, J. A. Molecular Model for the Solubilization of Membranes into Nanodisks by Styrene Maleic Acid Copolymers. *Biophys. J.* **2015**, *108*, 279−290.
(54) Dörr, J. M.; Koorengevel, M. C.; Schäfer, M.; Prokofyev, A. V.; Scheidelaar, S.; Van Der Cruijsen, E. A. W.; Dafforn, T. R.; Baldus, M.; Killian, J. A. Detergent-free isolation, characterization, and functional reconstitution of a tetrameric K+ channel: The power of native nanodiscs. *Proc. Natl. Acad. Sci. U.S.A.* **2014**, *111*, 18607−18612.
(55) Doyle, M. T.; Jimah, J. R.; Dowdy, T.; Ohlemacher, S. I.; Larion, M.; Hinshaw, J. E.; Bernstein, H. D. Cryo-EM structures reveal multiple stages of bacterial outer membrane protein folding. *Cell* **2022**, *185*, 1143−1156.e13.
(56) Kaur, R.; Mangiafesto, J.; Pryharski, K.; Rasam, S.; Zagursky, R.; Pichichero, M. Expression conditions and characterization of a novelly constructed lipoprotein intended as a vaccine to prevent human Haemophilus influenzae infections. *J. Biol. Chem.* **2023**, *299* (8), No. 105031, DOI: 10.1016/j.jbc.2023.105031.
(57) Smith, A. A. A.; Autzen, H. E.; Faust, B.; Mann, J. L.; Muir, B. W.; Howard, S.; Postma, A.; Spakowitz, A. J.; Cheng, Y.; Appel, E. A. Lipid Nanodiscs via Ordered Copolymers. *Chem* **2020**, *6*, 2782−2795.
(58) Zalucki, Y. M.; Jen, F. E. C.; Pegg, C. L.; Nouwens, A. S.; Schulz, B. L.; Jennings, M. P. Evolution for improved secretion and fitness may be the selective pressures leading to the emergence of two NDM alleles. *Biochem. Biophys. Res. Commun.* **2020**, *524*, 555−560.
(59) Wagner, S.; Klepsch, M. M.; Schlegel, S.; Appel, A.; Draheim, R.; Tarry, M.; Högbom, M.; Van Wijk, K. J.; Slotboom, D. J.; Persson, J. O.; De Gier, J. W. Tuning *Escherichia coli* for membrane protein overexpression. *Proc. Natl. Acad. Sci. U.S.A.* **2008**, *105*, 14371−14376.
(60) Asmar, A. T.; Collet, J. F. Lpp, the Braun lipoprotein, turns 50—major achievements and remaining issues. *FEMS Microbiol. Lett.* **2018**, *365*, No. 199.
(61) Narita, S. I.; Tokuda, H. Overexpression of LolCDE allows deletion of the *Escherichia coli* gene encoding apolipoprotein N-acyltransferase. *J. Bacteriol.* **2011**, *193*, 4832−4840.
(62) Stewart, A. C.; Bethel, C. R.; Vanpelt, J.; Bergstrom, A.; Miller, C. G.; Williams, C.; Poth, R.; Morris, M.; Nix, J. C.; Tierney, D. L.; Page, R. C.; Crowder, M. W.; Bahr, G.; Vitor-horen, L.; Bethel, C. R.; Bonomo, R. A.; González, L. J. Clinical Evolution of New Delhi Metallo-β-Lactamase (NDM) Optimizes Resistance under Zn(II) Deprivation. *Antimicrob. Agents Chemother.* **2018**, *62* (1), No. e01849-17, DOI: 10.1128/AAC.01849-17.
(63) Capdevila, D. A.; Rondón, J. J.; Edmonds, K. A.; Rocchio, J. S.; Dujovne, M. V.; Giedroc, D. P. Bacterial Metallostasis: Metal Sensing, Metalloproteome Remodeling, and Metal Trafficking. *Chem. Rev.* **2024**, *124*, 13574−13659.
(64) Stephenson, J. L.; McGee, W. M.; Kronewitter, S. R.; Neil, J. R. Analysis of Intact Resistance Markers for Metallo-b-Lactamases in Bacterial Pathogens (Poster) *American Society for Mass Spectrometry (ASMS) Annual Conference* 2021.
(65) Buddelmeijer, N. The molecular mechanism of bacterial lipoprotein modification-How, when and why? *FEMS Microbiol. Rev.* **2015**, *39*, 246−261.
(66) Sun, Z.; Hu, L.; Sankaran, B.; Prasad, B. V. V.; Palzkill, T. Differential active site requirements for NDM-1 β-lactamase hydrolysis of carbapenem versus penicillin and cephalosporin antibiotics. *Nat. Commun.* **2018**, *9*, No. 4524, DOI: 10.1038/s41467-018-06839-1.
(67) Sadeghi, P.; Mahnam, K.; Salari-Jazi, A.; Aspatwar, A.; Faghri, J. Evolutionary trajectories of beta-lactamase NDM and DLST cluster in *Pseudomonas aeruginosa*: finding the putative ancestor. *Pathog. Global Health* **2023**, *118* (2), 170−181.
(68) De Seny, D.; Heinz, U.; Wommer, S.; Kiefer, M.; Meyer-Klaucke, W.; Galleni, M.; Frère, J. M.; Bauer, R.; Adolph, H. W. Metal Ion Binding and Coordination Geometry for Wild Type and Mutants of Metallo-β-lactamase from Bacillus cereus569/H/9 (BcII): A COMBINED THERMODYNAMIC, KINETIC, AND SPECTROSCOPIC APPROACH. *J. Biol. Chem.* **2001**, *276*, 45065−45078.
(69) Wommer, S.; Rival, S.; Heinz, U.; Galleni, M.; Frère, J. M.; Franceschini, N.; Amicosante, G.; Rasmussen, B.; Bauer, R.; Adolph, H. W. Substrate-activated Zinc Binding of Metallo-β-lactamases: PHYSIOLOGICAL IMPORTANCE OF THE MONONUCLEAR ENZYMES. *J. Biol. Chem.* **2002**, *277*, 24142−24147.
(70) Jacquin, O.; Balbeur, D.; Damblon, C.; Marchot, P.; De Pauw, E.; Roberts, G. C. K.; Frère, J. M.; Matagne, A. Positively Cooperative Binding of Zinc Ions to Bacillus cereus 569/H/9 β-Lactamase II Suggests that the Binuclear Enzyme Is the Only Relevant Form for Catalysis. *J. Mol. Biol.* **2009**, *392*, 1278−1291.
(71) Hemmingsen, L.; Damblon, C.; Antony, J.; Jensen, M.; Werner Adolph, H.; Wommer, S.; Roberts, G. C. K.; Bauer, R. Dynamics of mononuclear cadmium β-lactamase revealed by the combination of NMR and PAC spectroscopy. *J. Am. Chem. Soc.* **2001**, *123*, 10329−10335.
(72) Thomas, P. W.; Cho, E. J.; Bethel, C. R.; Smisek, T.; Ahn, Y.; Schroeder, J. M.; Thomas, C. A.; Dalby, K. N.; Beckham, J. T.; Crowder, M. W.; Bonomo, R. A.; Fast, W. Discovery of an Effective Small-Molecule Allosteric Inhibitor of New Delhi Metallo- β -lactamase (NDM). *ACS Infect. Dis.* **2022**, *8*, 811−824.
(73) Garau, G.; Bebrone, C.; Anne, C.; Galleni, M.; Frère, J. M.; Dideberg, O. A metallo-beta-lactamase enzyme in action: crystal

structures of the monozinc carbapenemase CphA and its complex with biapenem. *J. Mol. Biol.* **2005**, *345*, 785−795.
(74) Bebrone, C. Metallo-β-lactamases (classification, activity, genetic organization, structure, zinc coordination) and their superfamily. In *Biochem. Pharmacol.*; Elsevier Inc, 2007.
(75) López, C.; Delmonti, J.; Bonomo, R. A.; Vila, A. J. Deciphering the evolution of metallo-β-lactamases: A journey from the test tube to the bacterial periplasm. *J. Biol. Chem.* **2022**, *298*, No. 101665, DOI: 10.1016/j.jbc.2022.101665.
(76) Hall, B. G.; Salipante, S. J.; Barlow, M. Independent origins of subgroup B1 + B2 and subgroup B3 metallo-β-lactamases. *J. Mol. Evol* **2004**, *59*, 133−141.
(77) Palzkill, T. Metallo-β-lactamase structure and function. *Ann. N.Y. Acad. Sci.* **2013**, *1277*, 91.
(78) Teufel, F.; Almagro Armenteros, J. J.; Johansen, A. R.; Gíslason, M. H.; Pihl, S. I.; Tsirigos, K. D.; Winther, O.; Brunak, S.; von Heijne, G.; Nielsen, H. SignalP 6.0 predicts all five types of signal peptides using protein language models. *Nat. Biotechnol.* **2022**, *40*, 1023−1025.
(79) Niu, W.; Ti, R.; Li, D.; Dong, R.; Dong, J.; Ye, Y.; Xiao, Y.; Wang, Z. Structural insight into the subclass B1 metallo-β-lactamase AFM-1. *Biochem. Biophys. Res. Commun.* **2024**, *720*, No. 150102.
(80) Chen, M.; Cai, H.; Li, Y.; Wang, N.; Zhang, P.; Hua, X.; Yu, Y.; Sun, R. Plasmid-Borne AFM Alleles in Pseudomonas aeruginosa Clinical Isolates from China. *Microbiol. Spectr.* **2022**, *10*, No. e02035−22.
(81) Capodimonte, L.; Teixeira, F.; Meireles, P.; Bahr, G.; Bonomo, R. A.; Dal Peraro, M.; López, C.; Vila, A. J.; Yu, E. W. OXA β-lactamases from *Acinetobacter* spp. are membrane bound and secreted into outer membrane vesicles *mBio*; Yu, E. W. Ed.; 2024.

https://doi.org/10.1021/acs.biochem.5c00106
Biochemistry XXXX, XXX, XXX−XXX